

Bidirectional-Reachable Hierarchical Reinforcement Learning with Mutually Responsive Policies

Yu Luo

luoyu19@mails.tsinghua.edu.cn

Department of Computer Science and Technology
Tsinghua University

Fuchun Sun*

fcsun@tsinghua.edu.cn

Department of Computer Science and Technology
Tsinghua University

Tianying Ji

jity20@mails.tsinghua.edu.cn

Department of Computer Science and Technology
Tsinghua University

Xianyuan Zhan

zhanxianyuan@air.tsinghua.edu.cn

Institute for AI Industry Research
Tsinghua University

Abstract

Hierarchical reinforcement learning (HRL) addresses complex long-horizon tasks by skillfully decomposing them into subgoals. Therefore, the effectiveness of HRL is greatly influenced by subgoal reachability. Typical HRL methods only consider subgoal reachability from the unilateral level, where a dominant level enforces compliance to the subordinate level. However, we observe that when the dominant level becomes trapped in local exploration or generates unattainable subgoals, the subordinate level is negatively affected and cannot follow the dominant level’s actions. This can potentially make both levels stuck in local optima, ultimately hindering subsequent subgoal reachability. Allowing real-time bilateral information sharing and error correction would be a natural cure for this issue, which motivates us to propose a mutual response mechanism. Based on this, we propose the Bidirectional-reachable Hierarchical Policy Optimization (BrHPO)—a simple yet effective algorithm that also enjoys computation efficiency. Experiment results on a variety of long-horizon tasks showcase that BrHPO outperforms other state-of-the-art HRL baselines, coupled with a significantly higher exploration efficiency and robustness¹.

1 Introduction

Reinforcement learning (RL) has demonstrated impressive capabilities in decision-making scenarios, ranging from achieving superhuman performance in games (Mnih et al., 2015; Lample & Chaplot, 2017; Silver et al., 2018), developing complex skills in robotics (Levine et al., 2016; Schulman et al., 2015) and enabling smart policies in autonomous driving (Jaritz et al., 2018; Kiran et al., 2021; Cao et al., 2023). Most of these accomplishments are attributed to single-level methods (Sutton & Barto, 2018), which learn a flat policy by trial and error without extra task decomposition or subgoal guidance. While single-level methods excel at short-horizon tasks involving inherently atomic behaviors (Levy et al., 2018; Nachum et al., 2018b; Pateria et al., 2021b), they often struggle to optimize effectively in long-horizon complex tasks that require multi-stage reasoning or sparse reward signals. To address this challenge, hierarchical reinforcement learning (HRL) has been proposed, aiming to decompose complex tasks into a hierarchy of subtasks or skills (Kulkarni et al., 2016; Bacon et al., 2017; Vezhnevets et al., 2017). By exploiting subtask structure and acquiring reusable skills, HRL empowers agents to solve long-horizon tasks efficiently.

¹We have released our code here: <https://github.com/Roythuly/BrHPO>

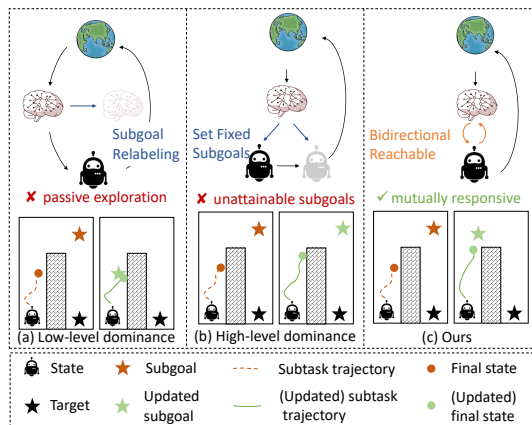


Figure 1: A motivating example of our proposed BrHPO. The earth, brain, and robot symbols stand for the environment, high-level policy, and low-level policy, respectively. We illustrate the behaviors of hierarchical policies before and after updated for each case. **Left:** Updated subgoal is limited by low-level exploration. **Middle:** Low-level policy struggles to approach the fixed subgoal. **Right:** hierarchical policies are mutually responsive for subgoal reachability.

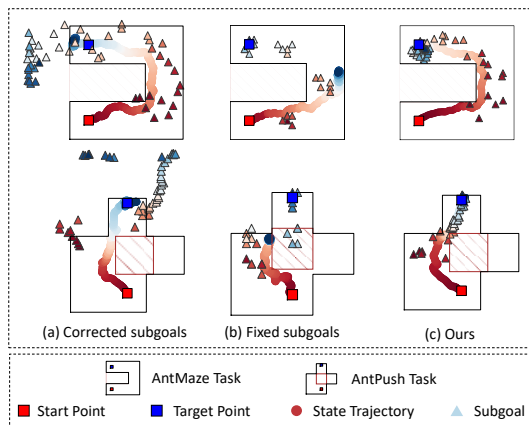


Figure 2: The state-subgoal trajectory comparison of baselines **HIRO** (a), **RIS** (b) and our **BrHPO** (c). We visualize the state trajectories (represented by the red-to-blue gradient lines) and the guided subgoals (represented by triangles). Note that lines and triangles of the same colour indicate that they belong to the same subtask. The results demonstrate that BrHPO can improve the alignment between states and subgoals, thus benefitting overall performance.

Subgoal-based HRL methods, a prominent paradigm in HRL, partition complex tasks into simpler subtasks by strategically selecting subgoals to guide exploration (Vezhnevets et al., 2017; Nachum et al., 2018b). Subgoal reachability, which is utilized as an intrinsic reward for exploration in different subtasks (Sukhbaatar et al., 2018), is crucial in evaluating how effectively the low-level policies’ exploration trajectory aligns with the high-level policy’s subgoal, ultimately determining task performance (Vezhnevets et al., 2017; Zhang et al., 2020). However, existing approaches for improving subgoal reachability predominantly focus on one level of the hierarchical policy, imposing dominance on the other level. This can be categorized as either low-level dominance or high-level dominance (Nachum et al., 2018b; Zhang et al., 2020; Andrychowicz et al., 2017; Chane-Sane et al., 2021; Eysenbach et al., 2019; Jurgenson et al., 2020). Low-level dominance (Figure 1a) refers to the accommodation of low-level passive exploratory behaviour by the high-level policy, causing the agent to get stuck near the starting position. On the other hand, high-level dominance (Figure 1b) may result in unattainable subgoals, causing repeated failure and sparse learning signals for the low-level policy. To assess these methods, we applied them to two HRL benchmarks, AntMaze and AntPush, and generated state-subgoal trajectories for visualization. The results reveal that the former methods exhibit lower exploration efficiency as the high level must generate distant subgoals to guide the low level (Figure 2a), while the latter methods may create unattainable subgoals, resulting in the low-level policy’s inability to track them (Figure 2b).

Enforcing subgoal reachability through unidirectional communication between the two levels has limitations in overall performance improvement. A bidirectional reachability approach, illustrated in Figure 1c, holds the potential to be more effective in HRL. From an optimization perspective, bidirectional reachability provides two key benefits: 1) *the high-level policy can generate subgoals that strike a balance between incentive and accessibility*, and 2) *the low-level policy can take more effective actions that drive subtask trajectories closer to the subgoal*. Despite its potential advantages, bidirectional subgoal reachability has not been extensively studied in previous research, and its effectiveness in enhancing HRL performance requires further investigation. We explore the theoretical benefits of bidirectional insights, and empirically demonstrate its effectiveness through visualizing the alignment between states and subgoals in Figure 2 and our ablation studies.

This paper aims to investigate the potential of bidirectional subgoal reachability in improving subgoal-based HRL performance, both theoretically and empirically. Specially, we propose a joint value function and then derive a performance difference bound for hierarchical policy optimization. The analysis suggests that enhancing subgoal reachability, from the mutual response of both-level policies, can effectively benefit overall performance. Motivated by these, our main contribution is a simple yet effective algorithm, Bidirectional-reachable Hierarchical Policy Optimization (BrHPO) which incorporates a mutual response mechanism to efficiently compute subgoal reachability and integrate it into hierarchical policy optimization. Through empirical evaluation, we demonstrate that BrHPO achieves promising asymptotic performance and exhibits superior training efficiency compared to state-of-the-art HRL methods. Additionally, we investigate different variants of BrHPO to showcase the effectiveness and robustness of the proposed mechanism.

2 Preliminaries

We consider an infinite-horizon discounted Markov Decision Process (MDP) with state space \mathcal{S} , action space \mathcal{A} , goal/subgoal space \mathcal{G} , unknown transition probability $P_{s,s'}^a : \mathcal{S} \times \mathcal{A} \times \mathcal{S} \rightarrow [0, 1]$, reward function $r : \mathcal{S} \times \mathcal{A} \times \mathcal{G} \rightarrow \mathbb{R}$, and discounted factor $\gamma \in (0, 1)$. The objective of RL is to find a policy $\pi : \mathcal{S} \rightarrow \Delta(\mathcal{A})$ to maximize the discounted cumulative reward from the environment, which can be formed as $\pi^* = \arg \max_{\pi} \mathbb{E}_{(s_t, a_t) \sim P, \pi} [\sum_{t=0}^{\infty} \gamma^t r(s_t, a_t)]$.

Subgoal-based HRL, also called Feudal HRL (Dayan & Hinton, 1992; Vezhnevets et al., 2017), comprises two hierarchies: a high-level policy generating subgoals, and a low-level policy pursuing subgoals in each subtask. Assume that each subtask contains a fixed length of k timesteps, allowing us to split the original task into multiple subtasks. Given the task goal \hat{g} , at the beginning of the i -th subtask where $i \in \mathbb{N}$, the high-level policy π_h observes state s_{ik} and then outputs a subgoal $g_{(i+1)k} \sim \pi_h(\cdot | s_{ik}, \hat{g}) \in \mathcal{G}$. Then, in each subtask, the low-level policy π_l performs actions conditioned on the subgoal and the current state, $a_{ik+j} \sim \pi_l(\cdot | s_{ik+j}, g_{(i+1)k}) \in \mathcal{A}$, where $j \in [0, k-1]$ is a pedometer in one single subtask. With the guidance from the subgoal, the state-subgoal-action trajectory in the i -th subtask comes out to be

$$\tau_i^{\pi_h, \pi_l} \triangleq \{(s_{ik+j} | s_{ik}, g_{(i+1)k} \sim \pi_h(\cdot | s_{ik}, \hat{g}), a_{ik+j} \sim \pi_l(\cdot | s_{ik+j}, g_{(i+1)k})\}_{j=0}^{k-1}, \quad (1)$$

and the whole task trajectory forms by stitching all subtask trajectories as $\tau = \cup_{i=0}^{\infty} (\tau_i^{\pi_h, \pi_l})$.

Following prior methods (Andrychowicz et al., 2017; Nachum et al., 2018b; Zhang et al., 2020), we optimize π_h based on the high-level reward r_h , defined as the environment reward feedback summated over a subtask

$$r_h(\tau_i^{\pi_h, \pi_l}) = r_h(s_{ik}, g_{(i+1)k}) = \sum_{j=0}^{k-1} r(s_{ik+j}, a_{ik+j}), \quad (2)$$

and the intrinsic reward for the low-level policy π_l is

$$r_l(s_{ik+j}, a_{ik+j}, g_{(i+1)k}) = -\mathcal{D}(\psi(s_{ik+j+1}), g_{(i+1)k}). \quad (3)$$

where $\psi : \mathcal{S} \mapsto \mathcal{G}$ is a pre-defined state-to-goal mapping function and $\mathcal{D} : \mathcal{G} \times \mathcal{G} \rightarrow \mathbb{R}_{\geq 0}$ is a chosen binary or continuous distance measurement (Zhang et al., 2022).

3 Bidirectional Subgoal Reachability in HRL

In this section, we introduce the concept of bidirectional subgoal reachability and highlight its differences from the previously studied unidirectional reachability. Specifically, bidirectional subgoal reachability considers the capacities of both high-level guidance and low-level exploration, allowing for more flexibility in HRL. We then discuss how this bidirectional reachability is integrated into the optimization objective of hierarchical policies, resulting in a mutual response mechanism. Finally, we present performance difference bounds associated with bi-directional reachability, providing valuable theoretical insights for subgoal-based HRL.

3.1 Bidirectional Subgoal Reachability

In contrast to previous unilateral subgoal reachability, termed as the high- or low-level dominance, our work aims to propose a bidirectional subgoal reachability metric that simultaneously considers the cooperation capacities of high-level guidance and low-level exploration within a single subtask.

Definition 3.1. The bidirectional subgoal reachability $\mathcal{R}_i^{\pi_h, \pi_l}$ at the i -th subtask is defined by

$$\mathcal{R}_i^{\pi_h, \pi_l} = \mathbb{E}_{g_{(i+1)k} \sim \pi_h, s_{(i+1)k} \sim \tau_i^{\pi_h, \pi_l}} \left[\mathcal{D}(\psi(s_{(i+1)k}), g_{(i+1)k}) / \mathcal{D}(\psi(s_{ik}), g_{(i+1)k}) \right]. \quad (4)$$

In this definition, subgoal reachability is equal to the ratio of the final distance (the final reached state $s_{(i+1)k}$ to the subgoal $g_{(i+1)k}$) to the initial distance (the initial state s_{ik} to the subgoal $g_{(i+1)k}$). Note that the smaller $\mathcal{R}_i^{\pi_h, \pi_l}$ means the better subgoal reachability and we define $\mathcal{R}_i^{\pi_h, \pi_l} = 0$ if $\mathcal{D}(\psi(s_{ik}), g_{(i+1)k}) = 0$. Although conceptually simple, this form has two benefits:

- When given the initial state s_{ik} of the sub-task, the subgoal reachability depends only on the final distance, and is independent of the intermediate exploration process, aligning with the properties of hierarchical abstraction. Besides, this is conducive to decoupling the guidance of the high-level policy and the exploration of the low-level policy, avoiding the issues of high- or low-level dominances;
- Using initial distance $\mathcal{D}(\psi(s_{ik}), g_{(i+1)k})$ as the regularization can eliminate the difference caused by the initial conditions of different sub-tasks. Thus, it can comprehensively measure whether the subgoal is easily reachable and whether the sub-task is easy to complete. For instance, a subgoal with an initial distance of 10 and a final distance of 3, although the final distance is larger, has a better subgoal reachability than a subgoal with an initial distance of 5 but a final distance 2.

In contrast to previous methods, such as using environmental dynamics (Zhang et al., 2020) or policy behavior (Nachum et al., 2018b; Kreidieh et al., 2019) for measuring subgoal reachability, our method is a continuous metric and can assess the cooperative effects of hierarchical policies rather than one of them. Therefore, improving subgoal reachability during policy optimization can be effective in enhancing the performance of hierarchical policies. Further, by recognizing that the low-level intrinsic reward shares the same form as the distance computation, we can replace the distance computation with the low-level reward. Thus, we can calculate the subgoal reachability by

$$\mathcal{R}_i^{\pi_h, \pi_l} = \mathbb{E}_{g_{(i+1)k} \sim \pi_h, s_{(i+1)k} \sim \tau_i^{\pi_h, \pi_l}} \left[\frac{\mathcal{D}(\psi(s_{(i+1)k}), g_{(i+1)k})}{\mathcal{D}(\psi(s_{ik}), g_{(i+1)k})} \right] = \mathbb{E}_{r_l \sim \tau_i^{\pi_h, \pi_l}} \frac{r_{l, (i+1)k}}{r_{l, ik}}. \quad (5)$$

Specifically, we use a temporary replay buffer for storing subtask trajectory $\tau_i^{\pi_h, \pi_l}$ upon subtask completion. Then, we can sample the first low-level reward $r_{l, ik} = r_l(s_{ik}, a_{ik}, g_{(i+1)k})$ and the last one $r_{l, (i+1)k} = r_l(s_{(i+1)k}, a_{(i+1)k}, g_{(i+1)k})$ from the temporary buffer to calculate the reachability. Notably, such a design is quite lightweight, incurring $O(1)$ computational complexity, without introducing additional training costs.

3.2 Bidirectional Reachability Hierarchical Policy Optimization

With the bidirectional subgoal reachability in hand, we turn to design the core mutual response mechanism, which aims at enhancing the reachability with the help of hierarchical policies.

High-level policy optimization. In our approach, we opt to use $\mathcal{R}_i^{\pi_h, \pi_l}$ as a regularization for optimizing π_h . During the high-level policy evaluation phase, we exclusively rely on rewards from the environment to iteratively compute Q-values, which ensures the accuracy of guidance performance evaluation. Furthermore, in the policy improvement phase, using $\mathcal{R}_i^{\pi_h, \pi_l}$ as the regularization explicitly constrains the high-level policy’s subgoal generation. This focus allows it to concern the

subgoal-reaching performance of the low-level policy within a subtask. Let $D_h = D_h \cup \{\tau_i^{\pi_h, \pi_l}\}$ be the high-level replay buffer, we evaluate the high-level policy by,

$$Q^{\pi_h}(s, g) = \arg \min_Q \frac{1}{2} \mathbb{E}_{s, g \sim D_h} [r_h(s, g) + \gamma \mathbb{E}_{s' \sim D_h, g' \sim \pi_h} Q^{\pi_h}(s', g') - Q^{\pi_h}(s, g)]^2, \quad (6)$$

and update the high-level policy by minimizing the expected KL-divergence with the reachability term as,

$$\pi_h = \arg \min_{\pi_h} \mathbb{E}_{s \sim D_h} [\text{D}_{KL}(\pi_h(\cdot|s) \| \exp(Q^{\pi_h}(s, g) - V^{\pi_h}(s))) + \lambda_1 \mathcal{R}_i^{\pi_h, \pi_l}], \quad (7)$$

where $V^{\pi_h}(s) = \mathbb{E}_{g \sim \pi_h(\cdot|s)} [Q^{\pi_h}(s, g) - \log \pi_h(\cdot|s)]$ is the high-level soft state value function and λ_1 is a weight factor. Thus, we can adjust the response of the high level through tuning λ_1 .

Low-level policy optimization. In contrast to high-level policy, we utilize $\mathcal{R}_i^{\pi_h, \pi_l}$ as a reward bonus for low-level policy. This approach is designed to enable π_l to simultaneously focus on both low-level rewards and subgoal reachability during subgoal exploration. To ensure the improvement of bidirectional subgoal reachability by low-level policy, we introduce subgoal reachability as well as the low-level reward, which is formulated as

$$\hat{r}_l(s_{ik+j}, a_{ik+j}, g_{(i+1)k}) = r_l(s_{ik+j}, a_{ik+j}, g_{(i+1)k}) - \lambda_2 \mathcal{R}_i^{\pi_h, \pi_l}. \quad (8)$$

Let $D_l = D_l \cup \{(s, g, a, \hat{r}_l, s', g)\}$ be the low-level replay buffer. With the surrogate low-level reward established, the evaluation and optimization of low-level policy can be performed by

$$Q^{\pi_l}(s, a) = \arg \min_Q \frac{1}{2} \mathbb{E}_{s, g, a \sim D_l} [\hat{r}_l(s, a, g) + \gamma \mathbb{E}_{s' \sim D_l, a' \sim \pi_l} Q^{\pi_l}(s', a') - Q^{\pi_l}(s, a)]^2, \quad (9)$$

$$\pi_l = \arg \min_{\pi_l} \mathbb{E}_{s, g \sim D_l} [\text{D}_{KL}(\pi_l(\cdot|s, g) \| \exp(Q^{\pi_l}(s, a) - V^{\pi_l}(s)))]. \quad (10)$$

3.3 Theoretical Insights

The previous subsection proposes an optimization algorithm for high- and low-level policies based on bidirectional subgoal reachability, and we investigate how this algorithm works in this section. First, to evaluate the overall performance of HRL, we construct a joint value function by calculating the discounted summation of step-wise rewards accumulated along the trajectory generated by both the high- and low-level policies, as presented below:

Definition 3.2 (Joint Value Function of Hierarchical Policies). The long-term cumulative return $V^{\pi_h, \pi_l}(s_0)$ of the subgoal-based HRL in the real environment can be defined as,

$$\begin{aligned} V^{\pi_h, \pi_l}(s_0) &= \sum_t \gamma^t \mathbb{E}_{s, a \sim \mathbb{P}_t^{\pi_l, g}(\cdot, \cdot | s_0), g \sim \pi_h(\cdot | s)} [r(s_t, a_t, \hat{g})] \\ &= \sum_{i=0}^{\infty} \mathbb{E}_{g \sim \pi_h(\cdot | s)} \left[\gamma^{ik} \left(\sum_{j=0}^{k-1} \gamma^j \mathbb{E}_{s, a \sim \mathbb{P}_{ik+j}^{\pi_l, g}(\cdot, \cdot | s_0)} r(s_{ik+j}, a_{ik+j}, \hat{g}) \right) \right]. \end{aligned} \quad (11)$$

To investigate the optimality of the policies, we derive a performance difference bound between an induced optimal hierarchical policy $\Pi^* = \{\pi_h^*, \pi_l^*\}$ and a learned one $\Pi = \{\pi_h, \pi_l\}$, which can be formulated as $V^{\Pi^*}(s) - V^{\Pi}(s) \leq C$.

Theorem 3.3 (Sub-optimal performance difference bound of HRL). *The performance difference bound C between the induced optimal hierarchical policies Π^* and the learned one Π can be*

$$C(\pi_h, \pi_l) = \frac{2r_{max}}{(1-\gamma)^2} \left[\underbrace{\left((1+\gamma) \mathbb{E}_{g \sim \pi_h} \left(1 + \frac{\pi_h^*}{\pi_h} \right) \epsilon_{\pi_l^*, \pi_l}^g \right)}_{(i) \text{ hierarchical policies' inconsistency}} + \underbrace{2(\mathcal{R}_{max}^{\pi_h, \pi_l} + 2\gamma^k)}_{(ii) \text{ subgoal reachability penalty}} \right], \quad (12)$$

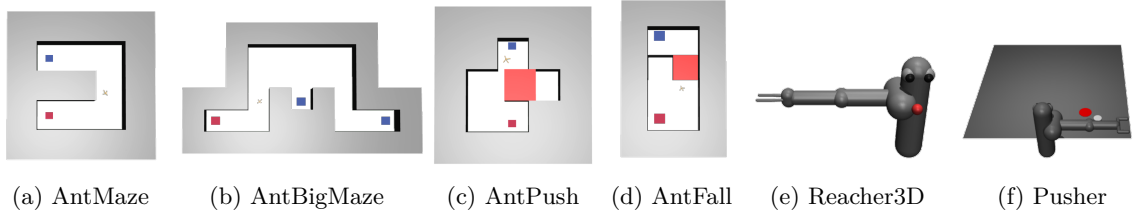


Figure 3: Environments used in our experiments. In maze tasks, the red square indicates the start point and the blue square represents the target point. In manipulation tasks, a robotic arm aims to make its end-effector and (puck-shaped) grey object reach the target position, which is marked as a red ball, respectively.

where $\epsilon_{\pi_l^*, \pi_l}^g$ is the distribution shift between π_l^* and π_l , and $\mathcal{R}_{max}^{\pi_h, \pi_l}$ is the maximum subgoal reachability penalty from the learned one Π , both of which are formulated as,

$$\epsilon_{\pi_l^*, \pi_l}^g = \max_{s \in \mathcal{S}, g \sim \pi_h} D_{TV}(\pi_l^*(\cdot|s, g) \| \pi_l(\cdot|s, g)) \quad \text{and} \quad \mathcal{R}_{max}^{\pi_h, \pi_l} = \max_{i \in \mathbb{N}} \mathcal{R}_i^{\pi_h, \pi_l}.$$

Please refer to Appendix A.1 for the detailed proof. As shown in Equation (12), the performance difference bound consists of two parts: (i) hierarchical policies’ inconsistency and (ii) subgoal reachability penalty. Of these, the former indicates the difference between the currently learned hierarchical policies π_h and π_l and the optimal hierarchical policies π_h^* and π_l^* . Since $(1 + \pi_h^*/\pi_h)$ and $\epsilon_{\pi_l^*, \pi_l}^g$ are decoupled from each other, this inspires us to optimize the high and low hierarchical policies separately to reduce the policies’ inconsistency and improve the performance of the policies. More importantly, the core difference from previous work is that the subgoal reachability penalty matters, which requires reduction from both high- and low-level policies, thus we integrate it into the optimization procedures of the two levels.

4 Experiment

Our experimental evaluation aims to investigate the following questions: 1) How does BrHPO’s performance on long-term goal-conditioned benchmark tasks compare to that of state-of-the-art counterparts in terms of sample efficiency and asymptotic performance? 2) How effective is the mutual response mechanism in enhancing subgoal reachability and improving performance?

Experimental setup We evaluate BrHPO on two categories of challenging long-horizon continuous control tasks, which feature both *dense* and *sparse* environmental reward, as illustrated in Figure 3. In the maze navigation environments, the reward is determined by the negative \mathcal{L}_2 distance between the current state and the target position within the goal space. In the robotics manipulation environments with sparse rewards, the reward is set to 0 when the distance is below a predefined threshold; otherwise, it’s set to -1 . Task success is defined as achieving a final distance to the target point of $d \leq 5$ for the maze tasks and $d \leq 0.25$ for the manipulation tasks. To ensure a fair comparison, all agents are initialized at the same position, eliminating extra environmental information introduction from random initialization (Lee et al., 2022). Detailed settings can be found in Appendix B.

4.1 Comparative evaluation

We compared BrHPO with the following baselines. 1) *HIRO* (Nachum et al., 2018b): designed an off-policy correction mechanism which required high-level experience to obey the current low-level policy; 2) *HIGL* (Kim et al., 2021): relied on the off-policy correction mechanism and introduced a k -step adjacent constraint (Zhang et al., 2020) and the novelty to discover appropriate subgoals; 3) *RIS* (Chane-Sane et al., 2021): utilized the hindsight method to generate the least-cost middle

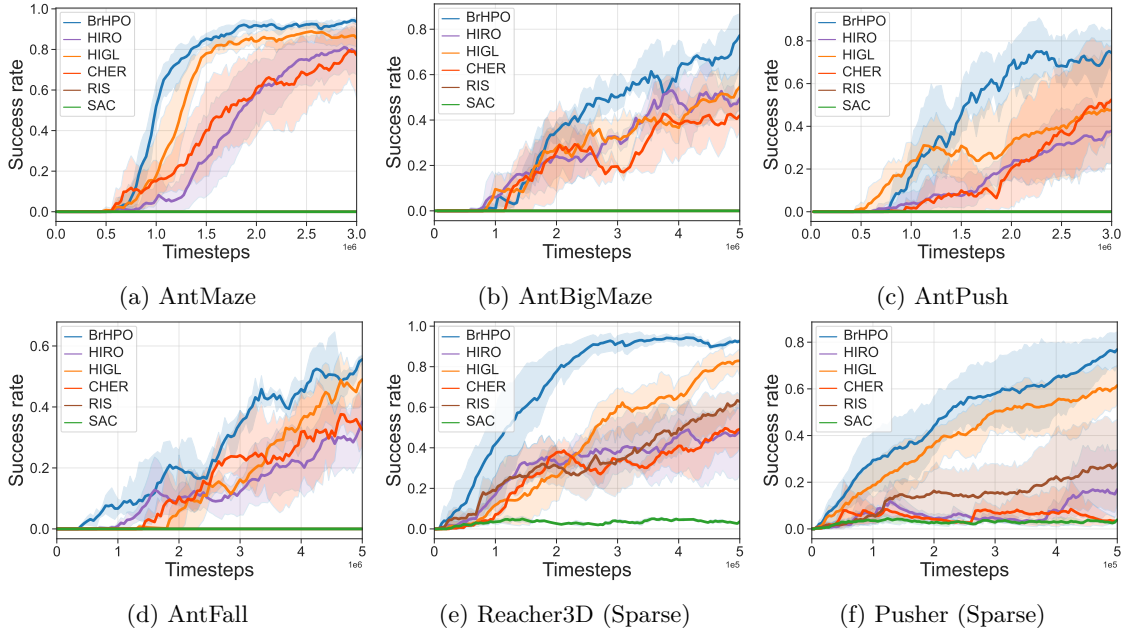


Figure 4: The average success rate in various continuous control tasks of BrHPO and baselines. The solid lines are the average success rate, while the shades indicate the standard error of the average performance. All algorithms are evaluated with 5 random seeds.

points as subgoals, forcing the low-level policy to follow the given subgoals; 4) *CHER* (Kreidieh et al., 2019): considered the cooperation of hierarchical policies, and the high-level policy needs to care about the low-level behaviour per step; 5) *SAC* (Haarnoja et al., 2018b): served as a benchmark of flat off-policy model-free algorithm and was applied as the backbone of BrHPO. Simply put, HIRO and HIGL focused on low-level domination, and RIS focused on high-level domination. CHER also considers the cooperation of different level policies while it requires step-by-step consideration.

The learning curves of BrHPO and the baselines across all tasks are plotted in Figure 4. Overall, the results demonstrate that BrHPO outperforms all baselines both in exploration efficiency and asymptotic performance. In particular, when dealing with large-scale (AntBigMaze) and partially-observed environments (AntPush and AntFall), BrHPO achieves better exploration and training stability, benefitting from the mutual response mechanism with information sharing and error correction for both levels. In contrast, acceptable baselines like HIRO, HIGL and CHER exhibit performance fluctuations and low success rates. It’s worth noting that BrHPO can handle *sparse* reward environments without any reward shaping or hindsight relabeling modifications, indicating that our proposed mechanism can capture serendipitous success and provide intrinsic guidance. Besides, we report the training wall-time in Appendix C.1, indicating that our method can achieve efficient computational performance, with training times comparable to a flat SAC policy. Notably, compared to previous approaches that utilize adjacency matrices (HRAC) or graphs to model subgoal reachability (HIGL), our method achieves at least a **2x** improvement in training efficiency with performance guarantee.

4.2 Ablation study

Next, we make ablations and modifications to our method to validate the effectiveness and robustness of the mechanism we devised.

Ablation on design choices. To investigate the effectiveness of each component, we compared BrHPO with several variants through AntMaze and AntPush tasks. The BrHPO variants include,

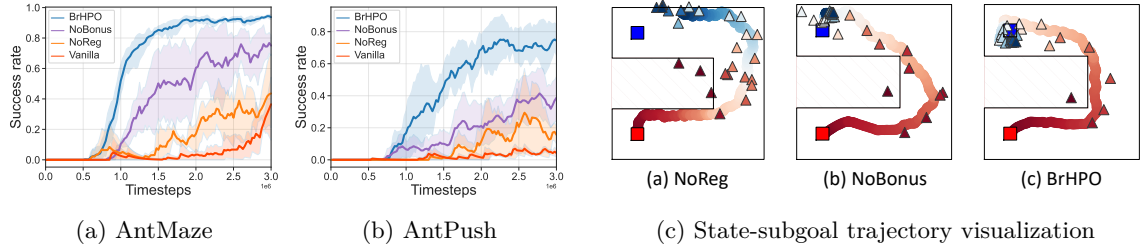
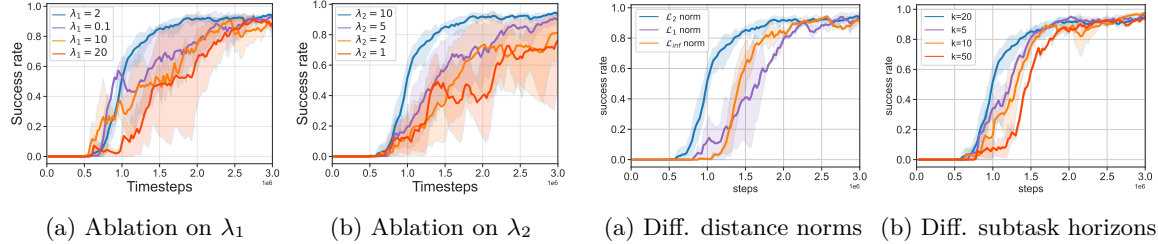


Figure 5: The performance and state-subgoal trajectory visualization from different BrHPO variants.

Figure 6: The learning curves with different weight factors λ_1 and λ_2 by AntMaze task.Figure 7: The learning curves from different \mathcal{D} and k to verify the robustness of the mechanism.

1) *Vanilla*, which removes the mutual response mechanism in both-level policies, resulting in π_h and π_l being trained solely by conventional SAC; 2) *NoReg*, which keeps the low-level reward bonus but disables the regularization term in high-level policy training; 3) *NoBonus*, where only the high-level policy concerns subgoal reachability but the low-level reward bonus is removed.

The learning curves and state-subgoal trajectory visualizations from different variants are presented in Figure 5. BrHPO outperforms all three variants by a significant margin, highlighting the importance of the mutual response mechanism at both levels. Interestingly, the *NoBonus* variant achieves better performance than the *NoReg* variant, suggesting that the subgoal reachability addressed by the high-level policy has a greater impact on overall performance. This observation is further supported by the trajectory visualization results.

Hyperparameters. We empirically studied the sensitivity of weight factors λ_1 and λ_2 in Figure 6. The results show that λ_1 and λ_2 within a certain range are acceptable. Upon closer analysis, we observed that when λ_1 is too small, the regularization term in high-level policy optimization has minimal influence. Consequently, the high-level policy tends to disregard the performance of the low-level policy during tuning, resembling a high-level dominance scenario. Conversely, when λ_1 is too large, the high-level policy overly prioritizes subgoal reachability, diminishing its exploration capability and resembling a low-level dominance scenario. These observations validate the effectiveness of the mutual response mechanism in maintaining a balanced interaction between the high- and low-level policies. Additionally, the results for λ_2 suggest that a larger value can generally improve subgoal reachability from the perspective of the low-level policy, leading to performance improvements and enhanced stability.

Robustness of mutual response mechanism. We conducted additional experiments on the AntMaze task to verify the robustness of the proposed mechanism. The computation of subgoal reachability, a key factor in the mutual response mechanism, depends on the choice of the distance measurement \mathcal{D} and the subtask horizon k . To test the distance measurement \mathcal{D} , we compared three distance functions: \mathcal{L}_2 norm, \mathcal{L}_∞ norm, and \mathcal{L}_1 norm. Figure 7a shows that our method performs well regardless of the distance function used, highlighting the adaptability of the proposed mechanism. Additionally, we varied the subtask horizon by setting $k = 5, 10, 20, 50$ (Figure 7b).

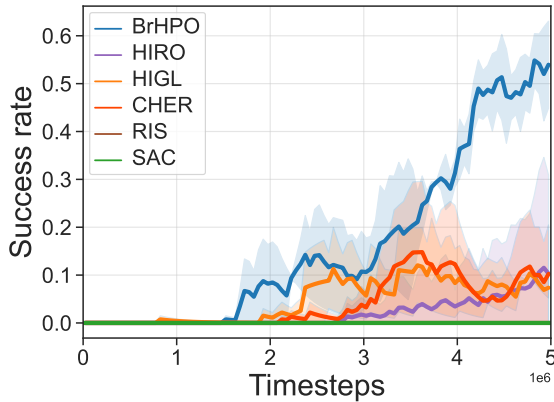
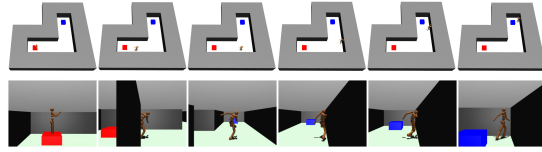
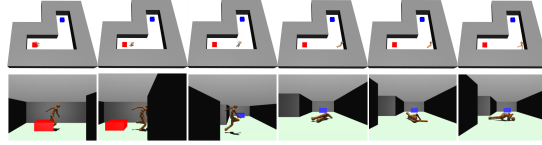


Figure 8: Learning curves of all methods. Mean and std by 4 runs.



(a) Visualization of BrHPO.



(b) Visualization of HIRO.

Figure 9: The behavior comparison between BrHPO and HIRO by HumanoidMaze.

Surprisingly, we achieved success rates of around 0.9 with different subtask horizons, indicating that the performance is robust to variations in the subtask horizon, only with a slight effect on the convergence speed during training. This flexibility of BrHPO in decoupling the high- and low-level horizons without the need for extra graphs, as required in DHRL (Lee et al., 2022), is noteworthy. More ablations by Reacher3D task are provided in Figure 12 of Appendix C.

In addition to evaluating parametric robustness, we subjected BrHPO to testing in stochastic environments to further evaluate its robustness. As depicted in Figure 13 of Appendix C, we introduce varying levels of Gaussian noise into the state space. The results demonstrate our BrHPO can effectively mitigate the impact of noise and ensure consistent final performance.

Mutual response mechanism in complex tasks. Except for the main results, we consider a more complex robot in a maze, HumanoidMaze, to further evaluate the mutual response mechanism. In this task, the simulated humanoid, where the state space contains **274** dimensions and the action space is **17**, needs to maintain body balance while being guided by the subgoal from the high-level policy. Consequently, the low-level policy necessitates extensive training to facilitate the humanoid’s ability to learn how to walk proficiently. This training process requires the high-level policy to exhibit “patience”, gradually adjusting the subgoals to guide the humanoid’s progress effectively. Figure 8 demonstrates the performance comparison, which showcases the superior advantage of BrHPO over HIRO. We additionally visualize the trajectory in Figure 9. We find that, our mutual response mechanism can encourage cooperation between the high- and the low-level policies, while the erroneous guidance from HIRO makes it difficult for humanoid to maintain balance and easily fall, thus failing the task.

5 Related Works

Hierarchical Reinforcement Learning (HRL) methods have emerged as promising solutions for addressing long-horizon complex tasks, primarily due to the synergistic collaboration between high-level task division and low-level exploration (Jong et al., 2008; Haarnoja et al., 2018a; Nachum et al., 2019; Pateria et al., 2021b; Eppe et al., 2022). Generally, HRL methods can be broadly categorized into two groups, option-based HRL (Sutton et al., 1999; Precup et al., 1998; Zhang et al., 2021; Mannor et al., 2004) and subgoal-based HRL (Dayan & Hinton, 1992; Nachum et al., 2019; Campos et al., 2020; Li et al., 2021b; Islam et al., 2022), that highlights the scope of guidance provided by the high-level policy. The first avenue involves the use of options to model the policy-switching mechanism in long-term tasks, which provides guidance to the low-level policy on when to terminate the current subtask and transition to a new one (Machado et al., 2017; Zhang & Whiteson, 2019). In contrast,

the subgoal-based HRL avenue (Vezhnevets et al., 2017; Nachum et al., 2018a; Gürtler et al., 2021; Czechowski et al., 2021; Li et al., 2021a) focuses on generating subgoals in fixed horizon subtasks rather than terminal signals, and our work falls under this category. Notably, subgoal-based HRL approaches prioritize subgoal reachability as a means of achieving high performance (Stein et al., 2018; Paul et al., 2019; Li et al., 2020; Czechowski et al., 2021; Pateria et al., 2021a).

Various methods have been proposed to enhance subgoal reachability, from either the high-level or low-level perspectives. When the low level is considered to be dominant, several works have proposed relabeling or correcting subgoals based on the exploration capacity of the low-level policy. Examples include off-policy correction in HIRO (Nachum et al., 2018b) and hindsight relabeling in HER (Andrychowicz et al., 2017), RIS (Chane-Sane et al., 2021) and HAC (Levy et al., 2019). On the other hand, when the high-level dominates, subgoals are solved from given prior experience or knowledge, and the low-level policy is trained merely to track the given subgoals (Savinov et al., 2018; Huang et al., 2019; Eysenbach et al., 2019; Jurgenson et al., 2020). In contrast to the listed prior works, BrHPO proposes a mutual response mechanism for ensuring bidirectional reachability. SoRB (Eysenbach et al., 2019), for instance, constructs an environmental graph from the given replay buffer for high-level planning and uses the waypoints as subgoals. SGT (Jurgenson et al., 2020) adopts a divide-and-conquer mechanism to search intermediate subgoals from given trajectories.

Meanwhile, our method relates to previous research that encourages cooperation between the high-level policy and the low-level one, where they explored various techniques for modelling subgoal reachability, including k -step adjacency matrix (Ferns et al., 2004; Castro, 2020; Zhang et al., 2020) or state-subgoal graph (Zhang et al., 2018; Kim et al., 2021; Lee et al., 2022). However, these methods can be computationally intensive and conservative. Our proposed method provides a more computationally efficient and flexible approach to gain subgoal reachability. By avoiding an explicit representation of the state-subgoal adjacency, our method can be more easily deployed and applied to a variety of different environments.

6 Conclusion

In this work, we identify that bilateral information sharing and error correction have been long neglected in previous HRL works. This will potentially cause local exploration and unattainable subgoal generation, which hinders overall performance and sample efficiency. To address this issue, we delve into the mutual response of hierarchical policies, both theoretically and empirically, revealing the crucial role of the mutual response mechanism. Based on these findings, we proposed the Bidirectional-reachable Hierarchical Policy Optimization (BrHPO) algorithm. BrHPO not only matches the best HRL algorithms in asymptotic performance, but it also shines in low computational load. Although BrHPO offers many advantages, a main challenge is to design an appropriate low-level reward to compute the subgoal reachability, thus limiting the application in sparse low-level reward settings (Lee et al., 2022). Future work that merits investigation are integrating up-to-date reachability measurement for bidirectional subgoal reachability and policy optimization backbone to develop a strong HRL algorithm.

Acknowledgments

This work was done at Tsinghua University and supported by the National Science and Technology Major Project (2021ZD0113801). We appreciate the reviewers' generous help to improve our paper.

References

Rishabh Agarwal, Max Schwarzer, Pablo Samuel Castro, Aaron C Courville, and Marc Bellemare. Deep reinforcement learning at the edge of the statistical precipice. In *Advances in neural information processing systems*, 2021.

- Marcin Andrychowicz, Filip Wolski, Alex Ray, Jonas Schneider, Rachel Fong, Peter Welinder, Bob McGrew, Josh Tobin, OpenAI Pieter Abbeel, and Wojciech Zaremba. Hindsight experience replay. In *Advances in Neural Information Processing Systems*, 2017.
- Pierre-Luc Bacon, Jean Harb, and Doina Precup. The option-critic architecture. In *Proceedings of the AAAI conference on artificial intelligence*, 2017.
- Víctor Campos, Alexander Trott, Caiming Xiong, Richard Socher, Xavier Giró-i Nieto, and Jordi Torres. Explore, discover and learn: Unsupervised discovery of state-covering skills. In *International Conference on Machine Learning*, 2020.
- Zhong Cao, Kun Jiang, Weitao Zhou, Shaobing Xu, Huei Peng, and Diange Yang. Continuous improvement of self-driving cars using dynamic confidence-aware reinforcement learning. *Nature Machine Intelligence*, 5(2):145–158, 2023.
- Pablo Samuel Castro. Scalable methods for computing state similarity in deterministic markov decision processes. In *the AAAI Conference on Artificial Intelligence*, 2020.
- Elliot Chane-Sane, Cordelia Schmid, and Ivan Laptev. Goal-conditioned reinforcement learning with imagined subgoals. In *International Conference on Machine Learning*, 2021.
- Konrad Czechowski, Tomasz Odrzygóźdź, Marek Zbysiński, Michał Zawalski, Krzysztof Olejnik, Yuhuai Wu, Łukasz Kuciński, and Piotr Miłoś. Subgoal search for complex reasoning tasks. In *Advances in Neural Information Processing Systems*, 2021.
- Peter Dayan and Geoffrey E Hinton. Feudal reinforcement learning. In *Advances in Neural Information Processing Systems*, 1992.
- Manfred Eppe, Christian Gumbsch, Matthias Kerzel, Phuong DH Nguyen, Martin V Butz, and Stefan Wermter. Intelligent problem-solving as integrated hierarchical reinforcement learning. *Nature Machine Intelligence*, 4(1):11–20, 2022.
- Ben Eysenbach, Russ R Salakhutdinov, and Sergey Levine. Search on the replay buffer: Bridging planning and reinforcement learning. In *Advances in Neural Information Processing Systems*, 2019.
- Norm Ferns, Prakash Panangaden, and Doina Precup. Metrics for finite markov decision processes. In *UAI*, 2004.
- Nico Gürtler, Dieter Büchler, and Georg Martius. Hierarchical reinforcement learning with timed subgoals. In *Advances in Neural Information Processing Systems*, 2021.
- Tuomas Haarnoja, Kristian Hartikainen, Pieter Abbeel, and Sergey Levine. Latent space policies for hierarchical reinforcement learning. In *International Conference on Machine Learning*, 2018a.
- Tuomas Haarnoja, Aurick Zhou, Pieter Abbeel, and Sergey Levine. Soft actor-critic: Off-policy maximum entropy deep reinforcement learning with a stochastic actor. In *International Conference on Machine Learning*, 2018b.
- Zhiao Huang, Fangchen Liu, and Hao Su. Mapping state space using landmarks for universal goal reaching. In *Advances in Neural Information Processing Systems*, 2019.
- Riashat Islam, Hongyu Zang, Anirudh Goyal, Alex M Lamb, Kenji Kawaguchi, Xin Li, Romain Laroche, Yoshua Bengio, and Remi Tachet des Combes. Discrete compositional representations as an abstraction for goal conditioned reinforcement learning. In *Advances in Neural Information Processing Systems*, 2022.
- Michael Janner, Justin Fu, Marvin Zhang, and Sergey Levine. When to trust your model: Model-based policy optimization. In *Advances in neural information processing systems*, 2019.

- Maximilian Jaritz, Raoul De Charette, Marin Toromanoff, Etienne Perot, and Fawzi Nashashibi. End-to-end race driving with deep reinforcement learning. In *2018 IEEE International Conference on Robotics and Automation (ICRA)*, pp. 2070–2075. IEEE, 2018.
- Nicholas K Jong, Todd Hester, and Peter Stone. The utility of temporal abstraction in reinforcement learning. In *International Joint Conference on Autonomous Agents and Multiagent Systems*, 2008.
- Tom Jurgenson, Or Avner, Edward Groshev, and Aviv Tamar. Sub-goal trees a framework for goal-based reinforcement learning. In *International Conference on Machine Learning*, 2020.
- Sham Kakade and John Langford. Approximately optimal approximate reinforcement learning. In *International Conference on Machine Learning*, 2002.
- Junsu Kim, Younggyo Seo, and Jinwoo Shin. Landmark-guided subgoal generation in hierarchical reinforcement learning. In *Advances in Neural Information Processing Systems*, 2021.
- Diederik P Kingma and Jimmy Ba. Adam: A method for stochastic optimization. *arXiv preprint arXiv:1412.6980*, 2014.
- B Ravi Kiran, Ibrahim Sobh, Victor Talpaert, Patrick Mannion, Ahmad A Al Sallab, Senthil Yogamani, and Patrick Pérez. Deep reinforcement learning for autonomous driving: A survey. *IEEE Transactions on Intelligent Transportation Systems*, 23(6):4909–4926, 2021.
- Abdul Rahman Kreidieh, Glen Berseth, Brandon Trabucco, Samyak Parajuli, Sergey Levine, and Alexandre M Bayen. Inter-level cooperation in hierarchical reinforcement learning. *arXiv preprint arXiv:1912.02368*, 2019.
- Tejas D Kulkarni, Karthik Narasimhan, Ardavan Saeedi, and Josh Tenenbaum. Hierarchical deep reinforcement learning: Integrating temporal abstraction and intrinsic motivation. In *Advances in neural information processing systems*, 2016.
- Guillaume Lample and Devendra Singh Chaplot. Playing fps games with deep reinforcement learning. In *Proceedings of the AAAI Conference on Artificial Intelligence*, 2017.
- Seungjae Lee, Jigang Kim, Inkyu Jang, and H Jin Kim. Dhrl: A graph-based approach for long-horizon and sparse hierarchical reinforcement learning. In *Advances in Neural Information Processing Systems*, 2022.
- Sergey Levine, Chelsea Finn, Trevor Darrell, and Pieter Abbeel. End-to-end training of deep visuomotor policies. *The Journal of Machine Learning Research*, 17(1):1334–1373, 2016.
- Andrew Levy, George Konidaris, Robert Platt, and Kate Saenko. Learning multi-level hierarchies with hindsight. In *International Conference on Learning Representations*, 2018.
- Andrew Levy, George Konidaris, Robert Platt, and Kate Saenko. Learning multi-level hierarchies with hindsight. In *International Conference on Learning Representations*, 2019.
- Siyuan Li, Lulu Zheng, Jianhao Wang, and Chongjie Zhang. Learning subgoal representations with slow dynamics. In *International Conference on Learning Representations*, 2020.
- Siyuan Li, Jin Zhang, Jianhao Wang, Yang Yu, and Chongjie Zhang. Active hierarchical exploration with stable subgoal representation learning. In *International Conference on Learning Representations*, 2021a.
- Siyuan Li, Lulu Zheng, Jianhao Wang, and Chongjie Zhang. Learning subgoal representations with slow dynamics. In *International Conference on Learning Representations*, 2021b.
- Marlos C Machado, Marc G Bellemare, and Michael Bowling. A laplacian framework for option discovery in reinforcement learning. In *International Conference on Machine Learning*, 2017.

- Shie Mannor, Ishai Menache, Amit Hoze, and Uri Klein. Dynamic abstraction in reinforcement learning via clustering. In *International Conference on Machine Learning*, 2004.
- Volodymyr Mnih, Koray Kavukcuoglu, David Silver, Andrei A Rusu, Joel Veness, Marc G Bellemare, Alex Graves, Martin Riedmiller, Andreas K Fidjeland, Georg Ostrovski, et al. Human-level control through deep reinforcement learning. *nature*, 518(7540):529–533, 2015.
- Ofir Nachum, Shixiang Gu, Honglak Lee, and Sergey Levine. Near-optimal representation learning for hierarchical reinforcement learning. In *International Conference on Learning Representations*, 2018a.
- Ofir Nachum, Shixiang Shane Gu, Honglak Lee, and Sergey Levine. Data-efficient hierarchical reinforcement learning. In *Advances in Neural Information Processing Systems*, 2018b.
- Ofir Nachum, Haoran Tang, Xingyu Lu, Shixiang Gu, Honglak Lee, and Sergey Levine. Why does hierarchy (sometimes) work so well in reinforcement learning? *arXiv preprint arXiv:1909.10618*, 2019.
- Shubham Pateria, Budhitama Subagdja, Ah-Hwee Tan, and Chai Quek. End-to-end hierarchical reinforcement learning with integrated subgoal discovery. *IEEE Transactions on Neural Networks and Learning Systems*, 2021a.
- Shubham Pateria, Budhitama Subagdja, Ah-hwee Tan, and Chai Quek. Hierarchical reinforcement learning: A comprehensive survey. *ACM Computing Surveys*, 54(5):1–35, 2021b.
- Sujoy Paul, Jeroen Vanbaaar, and Amit Roy-Chowdhury. Learning from trajectories via subgoal discovery. In *Advances in Neural Information Processing Systems*, 2019.
- Doina Precup, Richard S Sutton, and Satinder Singh. Theoretical results on reinforcement learning with temporally abstract options. In *Machine Learning: ECML-98: 10th European Conference on Machine Learning Chemnitz, Germany, April 21–23, 1998 Proceedings 10*, 1998.
- Nikolay Savinov, Alexey Dosovitskiy, and Vladlen Koltun. Semi-parametric topological memory for navigation. In *International Conference on Learning Representations*, 2018.
- John Schulman, Philipp Moritz, Sergey Levine, Michael Jordan, and Pieter Abbeel. High-dimensional continuous control using generalized advantage estimation. *arXiv preprint arXiv:1506.02438*, 2015.
- David Silver, Thomas Hubert, Julian Schrittwieser, Ioannis Antonoglou, Matthew Lai, Arthur Guez, Marc Lanctot, Laurent Sifre, Dhharshan Kumaran, Thore Graepel, et al. A general reinforcement learning algorithm that masters chess, shogi, and go through self-play. *Science*, 362(6419):1140–1144, 2018.
- Gregory J Stein, Christopher Bradley, and Nicholas Roy. Learning over subgoals for efficient navigation of structured, unknown environments. In *Conference on robot learning*, 2018.
- Sainbayar Sukhbaatar, Zeming Lin, Ilya Kostrikov, Gabriel Synnaeve, Arthur Szlam, and Rob Fergus. Intrinsic motivation and automatic curricula via asymmetric self-play. In *International Conference on Learning Representations*, 2018.
- Richard S Sutton and Andrew G Barto. *Reinforcement learning: An introduction*. MIT press, 2018.
- Richard S Sutton, Doina Precup, and Satinder Singh. Between mdps and semi-mdps: A framework for temporal abstraction in reinforcement learning. *Artificial intelligence*, 112(1-2):181–211, 1999.
- Alexander Sasha Vezhnevets, Simon Osindero, Tom Schaul, Nicolas Heess, Max Jaderberg, David Silver, and Koray Kavukcuoglu. Feudal networks for hierarchical reinforcement learning. In *International Conference on Machine Learning*, 2017.

- Amy Zhang, Sainbayar Sukhbaatar, Adam Lerer, Arthur Szlam, and Rob Fergus. Composable planning with attributes. In *International Conference on Machine Learning*, 2018.
- Jesse Zhang, Haonan Yu, and Wei Xu. Hierarchical reinforcement learning by discovering intrinsic options. In *International Conference on Learning Representations*, 2021.
- Shangdong Zhang and Shimon Whiteson. Dac: The double actor-critic architecture for learning options. *Advances in Neural Information Processing Systems*, 32, 2019.
- Tianren Zhang, Shangqi Guo, Tian Tan, Xiaolin Hu, and Feng Chen. Generating adjacency-constrained subgoals in hierarchical reinforcement learning. In *Advances in Neural Information Processing Systems*, 2020.
- Tianren Zhang, Shangqi Guo, Tian Tan, Xiaolin Hu, and Feng Chen. Adjacency constraint for efficient hierarchical reinforcement learning. *IEEE Transactions on Pattern Analysis and Machine Intelligence*, 2022.

A Theoretical Analysis

A.1 Omitted Proofs

Theorem A.1 (Sub-optimal performance difference bound of HRL). *The performance difference bound C between the induced optimal hierarchical policies Π^* and the learned one Π can be*

$$C(\pi_h, \pi_l) = \frac{2r_{max}}{(1-\gamma)^2} \left[\underbrace{(1+\gamma)\mathbb{E}_{g\sim\pi_h} \left(1 + \frac{\pi_h^*}{\pi_h}\right) \epsilon_{\pi_l^*, \pi_l}^g}_{(i) \text{ hierarchical policies' inconsistency}} + \underbrace{2(\mathcal{R}_{max}^{\pi_h, \pi_l} + 2\gamma^k)}_{(ii) \text{ subgoal reachability penalty}} \right], \quad (13)$$

where $\epsilon_{\pi_l^*, \pi_l}^g$ is the distribution shift between π_l^* and π_l , and $\mathcal{R}_{max}^{\pi_h, \pi_l}$ is the maximum subgoal reachability penalty from the learned one Π , both of which are formulated as,

$$\epsilon_{\pi_l^*, \pi_l}^g = \max_{s \in \mathcal{S}, g \sim \pi_h} D_{TV}(\pi_l^*(\cdot|s, g) \| \pi_l(\cdot|s, g)) \quad \text{and} \quad \mathcal{R}_{max}^{\pi_h, \pi_l} = \max_{i \in \mathbb{N}} \mathcal{R}_i^{\pi_h, \pi_l}.$$

Summary of proof. We first divide the bound into three parts, $V^{\Pi^*}(s) - V^{\Pi}(s) = \underbrace{V^{\pi_h^*, \pi_l^*}(s_0) - V^{\pi_h^*, \pi_l}(s_0)}_{L_1} + \underbrace{V^{\pi_h^*, \pi_l}(s_0) - V^{\pi_h, \pi_l^*}(s_0)}_{L_2} + \underbrace{V^{\pi_h, \pi_l^*}(s_0) - V^{\pi_h, \pi_l}(s_0)}_{L_3}$. Then, we find the similarity of L_1 and L_3 , both of which denote that under the same high-level policy (π_h^* in L_1 while π_h in L_3). By Performance Difference Lemma (Kakade & Langford, 2002), we have

$$L_1 + L_3 \leq \frac{2r_{max}}{(1-\gamma)^2} \mathbb{E}_{g\sim\pi_h} \left(1 + \frac{\pi_h^*}{\pi_h}\right) \epsilon_{\pi_l^*, \pi_l}^g. \quad (14)$$

For L_2 , we follow Zhang et al. (2022) and substitute equation (4). Then we have

$$L_2 \leq \frac{r_{max}}{(1-\gamma)^2} (\mathcal{R}_{max}^{\pi_h, \pi_l} + 2\gamma^k). \quad (15)$$

Thus, we take the results of Equations (14) and (15) and achieve the final bound.

Proof. To derive the performance difference bound between Π^* and Π , we first divide the bound into three terms,

$$\begin{aligned} V^{\Pi^*}(s_0) - V^{\Pi}(s_0) &= V^{\pi_h^*, \pi_l^*}(s_0) - V^{\pi_h, \pi_l}(s_0) \\ &= \underbrace{V^{\pi_h^*, \pi_l^*}(s_0) - V^{\pi_h^*, \pi_l}(s_0)}_{L_1} + \underbrace{V^{\pi_h^*, \pi_l}(s_0) - V^{\pi_h, \pi_l^*}(s_0)}_{L_2} + \underbrace{V^{\pi_h, \pi_l^*}(s_0) - V^{\pi_h, \pi_l}(s_0)}_{L_3}. \end{aligned} \quad (16)$$

Then, our proof can be obtained to by tackling L_1 , L_2 and L_3 , respectively.

- Derivation of L_1

By adding and subtracting the same term in L_1 , we obtain

$$\begin{aligned}
L_1 &= V^{\pi_h^*, \pi_l^*}(s_0) - \left[\tilde{V}_0^{\pi_h^*, \pi_l^*}(s_0) + \gamma^k \mathbb{E}_{g \sim \pi_h^*, s \sim \mathbb{P}_k^{\pi_l^*, g}(\cdot | s_0)} V^{\pi_h^*, \pi_l^*}(s_k) \right] \\
&\quad + \left[\tilde{V}_0^{\pi_h^*, \pi_l^*}(s_0) + \gamma^k \mathbb{E}_{g \sim \pi_h^*, s \sim \mathbb{P}_k^{\pi_l^*, g}(\cdot | s_0)} V^{\pi_h^*, \pi_l}(s_k) \right] - V^{\pi_h^*, \pi_l}(s_0) \\
&= \left[\tilde{V}_0^{\pi_h^*, \pi_l^*}(s_0) + \gamma^k \mathbb{E}_{g \sim \pi_h^*, s \sim \mathbb{P}_k^{\pi_l^*, g}(\cdot | s_0)} V^{\pi_h^*, \pi_l^*}(s_k) \right] \leftarrow \text{By Lemma A.3} \\
&\quad - \left[\tilde{V}_0^{\pi_h^*, \pi_l^*}(s_0) + \gamma^k \mathbb{E}_{g \sim \pi_h^*, s \sim \mathbb{P}_k^{\pi_l^*, g}(\cdot | s_0)} V^{\pi_h^*, \pi_l}(s_k) \right] \\
&\quad + \left[\tilde{V}_0^{\pi_h^*, \pi_l^*}(s_0) + \gamma^k \mathbb{E}_{g \sim \pi_h^*, s \sim \mathbb{P}_k^{\pi_l^*, g}(\cdot | s_0)} V^{\pi_h^*, \pi_l}(s_k) \right] \\
&\quad - \left[\tilde{V}_0^{\pi_h^*, \pi_l}(s_0) + \gamma^k \mathbb{E}_{g \sim \pi_h^*, s \sim \mathbb{P}_k^{\pi_l, g}(\cdot | s_0)} V^{\pi_h^*, \pi_l}(s_k) \right] \\
&= \underbrace{\gamma^k \mathbb{E}_{g \sim \pi_h^*, s \sim \mathbb{P}_k^{\pi_l^*, g}(\cdot | s_0)} \left[V^{\pi_h^*, \pi_l^*}(s_k) - V^{\pi_h^*, \pi_l}(s_k) \right]}_{\text{part a}} + \underbrace{\left[\tilde{V}_0^{\pi_h^*, \pi_l^*}(s_0) - \tilde{V}_0^{\pi_h^*, \pi_l}(s_0) \right]}_{\text{part b}} \\
&\quad + \underbrace{\gamma^k \left[\mathbb{E}_{g \sim \pi_h^*, s \sim \mathbb{P}_k^{\pi_l^*, g}(\cdot | s_0)} V^{\pi_h^*, \pi_l}(s_k) - \mathbb{E}_{g \sim \pi_h^*, s \sim \mathbb{P}_k^{\pi_l, g}(\cdot | s_0)} V^{\pi_h^*, \pi_l}(s_k) \right]}_{\text{part c}}. \tag{17}
\end{aligned}$$

Then, we can deal with the three parts one by one to obtain the derivation of L_1 . Note that, part b represents the performance discrepancy in the first subtask, caused by different low-level policies π_l^* and π_l . Thus, consider the policy shift of the low-level policies, we suppose

$$\epsilon_{\pi_l^*, \pi_l}^g = \max_{s \in \mathcal{S}, g \sim \pi_h} \text{D}_{TV}(\pi_l^*(\cdot | s, g) \| \pi_l(\cdot | s, g)). \tag{18}$$

Then, recall r_{max} to be the maximum environmental reward, i.e., $r \leq r_{max}$, we have

$$\begin{aligned}
\text{part b} &= \tilde{V}_0^{\pi_h^*, \pi_l^*}(s_0) - \tilde{V}_0^{\pi_h^*, \pi_l}(s_0) \\
&= \sum_{j=0}^{k-1} \mathbb{E}_{g_k \sim \pi_h^*, s, a \sim \mathbb{P}_j^{\pi_l^*, g}(\cdot | s_0)} [\gamma^j r(s_j, a_j, \hat{g})] - \sum_{j=0}^{k-1} \mathbb{E}_{g_k \sim \pi_h^*, s, a \sim \mathbb{P}_j^{\pi_l, g}(\cdot | s_0)} [\gamma^j r(s_j, a_j, \hat{g})] \\
&\leq \sum_{j=0}^{k-1} \mathbb{E}_{g_k \sim \pi_h^*} 2 [\gamma^j r(s_j, a_j, \hat{g})] \text{D}_{TV}(\mathbb{P}_j^{\pi_l^*, g}(\cdot | s_0) \| \mathbb{P}_j^{\pi_l, g}(\cdot | s_0)) \\
&\leq 2r_{max} \sum_{j=0}^{k-1} \mathbb{E}_{g_k \sim \pi_h^*} \gamma^j j \epsilon_{\pi_l^*, \pi_l}^g. \leftarrow \text{By Lemma A.4} \tag{19}
\end{aligned}$$

For part c, note that the joint value function can be bounded as $V^{\pi_h, \pi_l}(s_0) \leq r_{max}/(1-\gamma)$. We can apply Lemma A.4 to bound the discrepancy of the low-level policies, and have

$$\begin{aligned}
\text{part c} &= \gamma^k \left[\mathbb{E}_{g \sim \pi_h^*, s \sim \mathbb{P}_k^{\pi_l^*, g}(\cdot | s_0)} V^{\pi_h^*, \pi_l}(s_k) - \mathbb{E}_{g \sim \pi_h^*, s \sim \mathbb{P}_k^{\pi_l, g}(\cdot | s_0)} V^{\pi_h^*, \pi_l}(s_k) \right] \\
&= \gamma^k \int_{g \in \mathcal{G}} \int_{s \in \mathcal{S}} \pi_h^*(g | s_k) \left(\mathbb{P}_k^{\pi_l^*, g}(s | s_0) - \mathbb{P}_k^{\pi_l, g}(s | s_0) \right) V^{\pi_h^*, \pi_l}(s) ds dg \\
&\leq \frac{2\gamma^k r_{max}}{1-\gamma} \mathbb{E}_{g \sim \pi_h^*} \left[\text{D}_{TV}(\mathbb{P}_k^{\pi_l^*, g}(\cdot | s_0) \| \mathbb{P}_k^{\pi_l, g}(\cdot | s_0)) \right] \\
&\leq \frac{2\gamma^k r_{max}}{1-\gamma} \mathbb{E}_{g \sim \pi_h^*} k \epsilon_{\pi_l^*, \pi_l}^g, \tag{20}
\end{aligned}$$

At last, for part a, we can apply the same recursion every k step,

$$\begin{aligned}
\text{part a} &= \gamma^k \mathbb{E}_{g \sim \pi_h^*, s \sim \mathbb{P}_{2k}^{\pi_l^*, g}(\cdot | s_0)} \left[V^{\pi_h^*, \pi_l^*}(s_k) - V^{\pi_h^*, \pi_l}(s_k) \right] \\
&\leq \gamma^{2k} \mathbb{E}_{g \sim \pi_h^*, s \sim \mathbb{P}_{2k}^{\pi_l^*, g}(\cdot | s_0)} \left[V^{\pi_h^*, \pi_l^*}(s_{2k}) - V^{\pi_h^*, \pi_l}(s_{2k}) \right] \\
&\quad + 2r_{max} \sum_{j=k}^{2k-1} \mathbb{E}_{g \sim \pi_h^*} \gamma^j j \epsilon_{\pi_l^*, \pi_l}^g + \frac{2\gamma^{2k} r_{max}}{1-\gamma} \mathbb{E}_{g \sim \pi_h^*} 2k \epsilon_{\pi_l^*, \pi_l}^g. \tag{21}
\end{aligned}$$

Now, with the derivation of part a, part b and part c, we can combine these and repeat the recursion step for infinitely many times

$$\begin{aligned}
L_1 &= \text{part a} + \text{part b} + \text{part c} \\
&\leq 2r_{max} \sum_{j=0}^{k-1} \mathbb{E}_{g_k \sim \pi_h^*} \gamma^j j \epsilon_{\pi_l^*, \pi_l}^g + \frac{2\gamma^k r_{max}}{1-\gamma} \mathbb{E}_{g \sim \pi_h^*} k \epsilon_{\pi_l^*, \pi_l}^g \\
&\quad + 2r_{max} \sum_{j=k}^{2k-1} \mathbb{E}_{g_{2k} \sim \pi_h^*} \gamma^j j \epsilon_{\pi_l^*, \pi_l}^g + \frac{2\gamma^{2k} r_{max}}{1-\gamma} \mathbb{E}_{g \sim \pi_h^*} 2k \epsilon_{\pi_l^*, \pi_l}^g \\
&\quad + \gamma^{2k} \mathbb{E}_{g \sim \pi_h^*, s \sim \mathbb{P}_{2k}^{\pi_l^*, g}(\cdot | s_0)} \left[V^{\pi_h^*, \pi_l^*}(s_{2k}) - V^{\pi_h^*, \pi_l}(s_{2k}) \right] \\
&\quad \vdots \\
&\leq 2r_{max} \sum_{i=0}^{\infty} \sum_{j=0}^{k-1} \mathbb{E}_{g \sim \pi_h^*} \gamma^{(ik+j)} (ik+j) \epsilon_{\pi_l^*, \pi_l}^g + \frac{\gamma^{(i+1)k}}{1-\gamma} \mathbb{E}_{g \sim \pi_h^*} (i+1)k \epsilon_{\pi_l^*, \pi_l}^g \\
&\leq 2r_{max} \frac{1+\gamma}{(1-\gamma)^2} \mathbb{E}_{g \sim \pi_h^*} \epsilon_{\pi_l^*, \pi_l}^g. \tag{22}
\end{aligned}$$

Thus, we complete the derivation of L_1 .

- **Derivation of L_3**

Compared with L_1 , the term L_3 replaces the high-level policy from π_h^* to π_h . Thus, we directly can get L_3 from the results of L_1 as

$$L_3 \leq 2r_{max} \frac{1+\gamma}{(1-\gamma)^2} \mathbb{E}_{g \sim \pi_h} \epsilon_{\pi_l^*, \pi_l}^g. \tag{23}$$

- **Derivation of L_2**

Similar to the derivation of L_1 , by adding and subtracting the same term in L_2 , we have

$$\begin{aligned}
L_2 &= V^{\pi_h^*, \pi_l}(s_0) - \left[\tilde{V}_0^{\pi_h^*, \pi_l}(s_0) + \gamma^k \mathbb{E}_{g \sim \pi_h^*, s \sim \mathbb{P}_k^{\pi_l, g}(\cdot | s_0)} V^{\pi_h, \pi_l^*}(s_k) \right] \\
&\quad + \left[\tilde{V}_0^{\pi_h^*, \pi_l}(s_0) + \gamma^k \mathbb{E}_{g \sim \pi_h^*, s \sim \mathbb{P}_k^{\pi_l, g}(\cdot | s_0)} V^{\pi_h, \pi_l^*}(s_k) \right] - V^{\pi_h, \pi_l^*}(s_0) \\
&= \left[\tilde{V}_0^{\pi_h^*, \pi_l}(s_0) + \gamma^k \mathbb{E}_{g \sim \pi_h^*, s \sim \mathbb{P}_k^{\pi_l, g}(\cdot | s_0)} V^{\pi_h^*, \pi_l}(s_k) \right] \\
&\quad - \left[\tilde{V}_0^{\pi_h^*, \pi_l}(s_0) + \gamma^k \mathbb{E}_{g \sim \pi_h^*, s \sim \mathbb{P}_k^{\pi_l, g}(\cdot | s_0)} V^{\pi_h, \pi_l^*}(s_k) \right] \\
&\quad + \left[\tilde{V}_0^{\pi_h^*, \pi_l}(s_0) + \gamma^k \mathbb{E}_{g \sim \pi_h^*, s \sim \mathbb{P}_k^{\pi_l, g}(\cdot | s_0)} V^{\pi_h, \pi_l^*}(s_k) \right] \\
&\quad - \left[\tilde{V}_0^{\pi_h, \pi_l^*}(s_0) + \gamma^k \mathbb{E}_{g \sim \pi_h, s \sim \mathbb{P}_k^{\pi_l^*, g}(\cdot | s_0)} V^{\pi_h, \pi_l^*}(s_k) \right] \\
&= \underbrace{\gamma^k \mathbb{E}_{g \sim \pi_h^*, s \sim \mathbb{P}_k^{\pi_l, g}(\cdot | s_0)} \left[V^{\pi_h^*, \pi_l}(s_k) - V^{\pi_h, \pi_l^*}(s_k) \right]}_{\text{part d}} + \underbrace{\left[\tilde{V}_0^{\pi_h^*, \pi_l}(s_0) - \tilde{V}_0^{\pi_h, \pi_l^*}(s_0) \right]}_{\text{part e}} \\
&\quad + \underbrace{\gamma^k \left[\mathbb{E}_{g \sim \pi_h^*, s \sim \mathbb{P}_k^{\pi_l, g}(\cdot | s_0)} V^{\pi_h, \pi_l^*}(s_k) - \mathbb{E}_{g \sim \pi_h, s \sim \mathbb{P}_k^{\pi_l^*, g}(\cdot | s_0)} V^{\pi_h, \pi_l^*}(s_k) \right]}_{\text{part f}}. \tag{24}
\end{aligned}$$

According to Assumption A.5, we suppose $r(s_t, a_t, \hat{g}) = \mathbb{E}_{g \sim \pi_h, s, a \sim \mathbb{P}_t^{\pi_l, g}} r_l(s_t, a_t, g) / \mathcal{D}(g, \hat{g})$, thus we summate the k -step reward in the first subtask in part e as

$$\begin{aligned}
&\sum_{j=0}^{k-1} \mathbb{E}_{g \sim \pi_h, s, a \sim \mathbb{P}_j^{\pi_l, g}(\cdot, | s_0)} \left[\gamma^j r(s_j, a_j, \hat{g}) \right] \\
&= r(s_0, a_0, \hat{g}) \sum_{j=0}^{k-1} \mathbb{E}_{g \sim \pi_h, s, a \sim \mathbb{P}_j^{\pi_l, g}(\cdot, | s_0)} \left[\gamma^j \frac{r(s_j, a_j, \hat{g})}{r(s_0, a_0, \hat{g})} \right] \\
&= r(s_0, a_0, \hat{g}) \sum_{j=0}^{k-1} \mathbb{E}_{g \sim \pi_h, s, a \sim \mathbb{P}_j^{\pi_l, g}(\cdot, | s_0)} \left[\gamma^j \frac{r_l(s_j, a_j, g)}{\mathcal{D}(g, \hat{g})} \frac{\mathcal{D}(g, \hat{g})}{r_l(s_0, a_0, g)} \right] \\
&= r(s_0, a_0, \hat{g}) \sum_{j=0}^{k-1} \mathbb{E}_{g \sim \pi_h, s, a \sim \mathbb{P}_j^{\pi_l, g}(\cdot, | s_0)} \left[\gamma^j \frac{r_l(s_j, a_j, g)}{r_l(s_0, a_0, g)} \right]. \tag{25}
\end{aligned}$$

Since the low-level policy is trained as a goal-conditioned policy, we have $r_l(s_j, a_j, g) \leq r_l(s_k, a_k, g)$. And the summation in the first subtask can be

$$\begin{aligned}
&\sum_{j=0}^{k-1} \mathbb{E}_{g \sim \pi_h, s, a \sim \mathbb{P}_j^{\pi_l, g}(\cdot, | s_0)} \left[\gamma^j r(s_j, a_j, \hat{g}) \right] \\
&\leq r(s_0, a_0, \hat{g}) \sum_{j=0}^{k-1} \mathbb{E}_{g \sim \pi_h, s, a \sim \mathbb{P}_j^{\pi_l, g}(\cdot, | s_0)} \left[\gamma^j \frac{r_l(s_k, a_k, g)}{r_l(s_0, a_0, g)} \right] \\
&= r(s_0, a_0, \hat{g}) \frac{1 - \gamma^k}{1 - \gamma} \frac{r_l(s_k, a_k, g)}{r_l(s_0, a_0, g)}. \tag{26}
\end{aligned}$$

Thus, we let the fraction $\mathcal{R}_i^{\pi_h, \pi_l} = r_l(s_k, a_k, g)/r_l(s_0, a_0, g)$ be the subgoal reachability definition, and the part e in L_2 can be

$$\begin{aligned}
\text{part e} &= \tilde{V}_0^{\pi_h^*, \pi_l}(s_0) - \tilde{V}_0^{\pi_h, \pi_l^*}(s_0) \\
&= \sum_{j=0}^{k-1} \mathbb{E}_{g \sim \pi_h^*, s, a \sim \mathbb{P}_j^{\pi_l, g}(\cdot, \cdot | s_0)} [\gamma^j r(s_j, a_j, \hat{g})] - \sum_{j=0}^{k-1} \mathbb{E}_{g \sim \pi_h, s, a \sim \mathbb{P}_j^{\pi_l^*, g}(\cdot, \cdot | s_0)} [\gamma^j r(s_j, a_j, \hat{g})] \\
&\leq r(s_0, a_0, \hat{g}) \frac{1 - \gamma^k}{1 - \gamma} \mathcal{R}_0^{\pi_h^*, \pi_l} - \sum_{j=0}^{k-1} \mathbb{E}_{g \sim \pi_h, s, a \sim \mathbb{P}_j^{\pi_l^*, g}(\cdot, \cdot | s_0)} [\gamma^j r(s_j, a_j, \hat{g})] \\
&\leq r_{max} \frac{1 - \gamma^k}{1 - \gamma} \left(\mathcal{R}_0^{\pi_h, \pi_l} - \mathcal{R}_0^{\pi_h^*, \pi_l^*} \right) \quad \leftarrow \quad \Pi^* \text{ can achieve best subgoal reachability} \\
&\leq r_{max} \frac{1 - \gamma^k}{1 - \gamma} \mathcal{R}_0^{\pi_h, \pi_l}. \tag{27}
\end{aligned}$$

The penultimate inequality is based on the property of the induced optimal hierarchical policies. Compared with the learned π_h , Figure 3 shows that π_h^* can balance the subgoal reachability and the guidance, thus $\mathcal{R}_0^{\pi_h, \pi_l} \geq \mathcal{R}_0^{\pi_h^*, \pi_l}$ (note that the smaller \mathcal{R} implies the better subgoal reachability). And, the optimal policies Π^* can achieve the optimal subgoal reachability, i.e. $\mathcal{R}_0^{\pi_h^*, \pi_l^*} \leq \mathcal{R}_0^{\pi_h, \pi_l}$. Thus, we have $\left(\mathcal{R}_0^{\pi_h^*, \pi_l} - \mathcal{R}_0^{\pi_h, \pi_l} \right) \leq \left(\mathcal{R}_0^{\pi_h, \pi_l} - \mathcal{R}_0^{\pi_h^*, \pi_l^*} \right)$.

Then, we turn to part f in L_2 . Considering the upper bound of the joint value function, we have

$$\begin{aligned}
\text{part f} &= \gamma^k \left[\mathbb{E}_{g \sim \pi_h^*, s \sim \mathbb{P}_k^{\pi_l, g}(\cdot | s_0)} V^{\pi_h, \pi_l^*}(s_k) - \mathbb{E}_{g \sim \pi_h, s \sim \mathbb{P}_k^{\pi_l^*, g}(\cdot | s_0)} V^{\pi_h, \pi_l^*}(s_k) \right] \\
&\leq \gamma^k \int_{g \in \mathcal{G}} \int_{s \in \mathcal{S}} [\pi_h^*(g|s) - \pi_h(g|s)] \left[\mathbb{P}_k^{\pi_l, g}(s|s_0) - \mathbb{P}_k^{\pi_l^*, g}(s|s_0) \right] \frac{r_{max}}{1 - \gamma} ds dg \\
&\leq 2\gamma^k \int_{g \in \mathcal{G}} \int_{s \in \mathcal{S}} \frac{r_{max}}{1 - \gamma} ds dg \\
&= \frac{2\gamma^k r_{max}}{1 - \gamma}. \tag{28}
\end{aligned}$$

With the derivation of part e and part f, we deal with part d by the recursion each k -steps as

$$\begin{aligned}
\text{part d} &= \gamma^k \mathbb{E}_{g \sim \pi_h^*, s \sim \mathbb{P}_k^{\pi_l, g}(\cdot | s_0)} \left[V^{\pi_h^*, \pi_l}(s_k) - V^{\pi_h, \pi_l^*}(s_k) \right] \\
&\leq \gamma^{2k} \mathbb{E}_{g \sim \pi_h^*, s \sim \mathbb{P}_{2k}^{\pi_l, g}(\cdot | s_0)} \left[V^{\pi_h^*, \pi_l}(s_{2k}) - V^{\pi_h, \pi_l^*}(s_{2k}) \right] \\
&\quad + r_{max} \frac{\gamma^k - \gamma^{2k}}{1 - \gamma} \mathcal{R}_1^{\pi_h, \pi_l} + \frac{2\gamma^{2k} r_{max}}{1 - \gamma}. \tag{29}
\end{aligned}$$

Thus, we combine the result of part d, part e and part f to obtain the results of L_2 as

$$\begin{aligned}
L_2 &= \text{part d} + \text{part e} + \text{part f} \\
&\leq r_{max} \frac{1 - \gamma^k}{1 - \gamma} \mathcal{R}_0^{\pi_h, \pi_l} + r_{max} \frac{\gamma^k - \gamma^{2k}}{1 - \gamma} \mathcal{R}_1^{\pi_h, \pi_l} + \frac{2\gamma^k r_{max}}{1 - \gamma} + \frac{2\gamma^{2k} r_{max}}{1 - \gamma} \\
&\quad + \gamma^{2k} \mathbb{E}_{g \sim \pi_h^*, s \sim \mathbb{P}_{2k}^{\pi_l, g}(\cdot | s_0)} \left[V^{\pi_h^*, \pi_l}(s_{2k}) - V^{\pi_h, \pi_l^*}(s_{2k}) \right] \\
&\quad \vdots \\
&\leq r_{max} \sum_{i=0}^{\infty} \frac{(1 - \gamma^k) \gamma^{ik}}{1 - \gamma} \mathcal{R}_i^{\pi_h, \pi_l} + \frac{2\gamma^{(i+1)k}}{1 - \gamma} \\
&\leq \frac{r_{max}}{(1 - \gamma)^2} (\mathcal{R}_{max}^{\pi_h, \pi_l} + 2\gamma^k). \tag{30}
\end{aligned}$$

In the last inequality, we define

$$\mathcal{R}_{max}^{\pi_h, \pi_l} = \max_{i \in \mathbb{N}} \mathcal{R}_i^{\pi_h, \pi_l}. \quad (31)$$

Now, we have the results of L_1 , L_2 and L_3 . The performance difference bound between Π^* and Π can be obtained as

$$\begin{aligned} V^{\Pi^*}(s_0) - V^{\Pi}(s_0) &= L_1 + L_2 + L_3 \\ &\leq 2r_{max} \frac{1+\gamma}{(1-\gamma)^2} \mathbb{E}_{g \sim \pi_h^*} \epsilon_{\pi_l^*, \pi_l}^g + \frac{r_{max}}{(1-\gamma)^2} (\mathcal{R}_{max}^{\pi_h, \pi_l} + 2\gamma^k) \\ &\quad + 2r_{max} \frac{1+\gamma}{(1-\gamma)^2} \mathbb{E}_{g \sim \pi_h} \epsilon_{\pi_l^*, \pi_l}^g \\ &= \frac{2r_{max}}{(1-\gamma)^2} \left[(1+\gamma) \mathbb{E}_{g \sim \pi_h} \left(1 + \frac{\pi_h^*}{\pi_h} \right) \epsilon_{\pi_l^*, \pi_l}^g + 2 (\mathcal{R}_{max}^{\pi_h, \pi_l} + 2\gamma^k) \right]. \end{aligned} \quad (32)$$

And the proof is complete. \square

Proposition A.2 (Equivalence between π^* and Π^*). *With the k -step trajectory slicing and the alignment method, the performance of Π^* and π^* is equivalent, i.e., $V^{\pi^*}(s) = V^{\Pi^*}(s)$.*

Proof. According to the k -step trajectory slicing and the alignment method, the induced optimal hierarchical policies Π^* can be generated by aligning with the k -step trajectory slice derived by π^* , thus we have

$$\begin{aligned} g_{(i+1)k} &\sim \pi_h^*(\cdot | s_{ik}) = \mathbb{P}_k^{\pi^*}(s_{(i+1)k} | s_{ik}) \\ &= p(s_{ik}) \prod_{j=0}^{k-1} P(s_{ik+j+1} | s_{ik+j}, a_{ik+j}) \pi^*(a_{ik+j} | s_{ik+j}), \end{aligned} \quad (33)$$

$$a_{ik+j} \sim \pi_l^*(\cdot | s_{ik+j}, g_{(i+1)k}) = \pi^*(a_{ik+j} | s_{ik+j}). \quad (34)$$

Thus, the value function for π^* and the joint value function for Π^* can be

$$\begin{aligned} V^{\pi^*}(s_0) &= \sum_t \gamma^t \mathbb{E}_{s \sim p(s'|s, a), a \sim \pi^*} [r(s_t, a_t, \hat{g})] \\ &= \sum_{i=0}^{\infty} \sum_{j=0}^{k-1} \mathbb{E}_{s \sim p(s'|s, a), a \sim \pi^*} \gamma^{ik+j} [r(s_{ik+j}, a_{ik+j}, \hat{g})] \\ &= \sum_{i=0}^{\infty} \mathbb{E}_{g \sim \pi_h^*} \left\{ \gamma^{ik} \sum_{j=0}^{k-1} \mathbb{E}_{s \sim p(s'|s, a), a \sim \pi_l^*} \gamma^j [r(s_{ik+j}, a_{ik+j}, \hat{g})] \right\} \\ &= \sum_{i=0}^{\infty} \mathbb{E}_{g \sim \pi_h^*(\cdot | s)} \left[\gamma^{ik} \left(\sum_{j=0}^{k-1} \gamma^j \mathbb{E}_{s, a \sim \mathbb{P}_{ik+j}^{\pi_l^*, g}(\cdot, \cdot | s_0)} r(s_{ik+j}, a_{ik+j}, \hat{g}) \right) \right] \\ &= V^{\Pi^*}(s_0) \end{aligned} \quad (35)$$

Thus, through the k -step trajectory slicing and the alignment method, the performance of Π^* and π^* is equivalent. And the proof is complete. \square

A.2 Useful Lemma and Assumption

Lemma A.3 (Bellman Backup in HRL). *Consider that the joint value function can be decomposed by the summation of subtasks. Given the initial state s_{ik} at the i -th subtask, the Bellman Backup of*

HRL defined in each subtask can be

$$V^{\pi_h, \pi_l}(s_{ik}) = \tilde{V}_i^{\pi_h, \pi_l}(s_{ik}) + \gamma^k \mathbb{E}_{g \sim \pi_h, s \sim \mathbb{P}_{(i+1)k}^{\pi_l, g}(\cdot | s_{ik})} [V^{\pi_h, \pi_l}(s_{(i+1)k})], \quad (36)$$

where $\tilde{V}_i^{\pi_h, \pi_l}(s_{ik})$ is the the environment return of Π with the i -th subtask, formulated as

$$\tilde{V}_i^{\pi_h, \pi_l}(s_{ik}) = \sum_{j=0}^{k-1} \mathbb{E}_{g \sim \pi_h, s, a \sim \mathbb{P}_{ik+j}^{\pi_l, g}(\cdot, \cdot | s_{ik})} [\gamma^j r(s_{ik+j}, a_{ik+j}, \hat{g})]. \quad (37)$$

Proof. According to the decomposition of the joint value function $V^{\pi_h, \pi_l}(s)$, we have

$$\begin{aligned} V^{\pi_h, \pi_l}(s_0) &= \sum_{i=0}^{\infty} \mathbb{E}_{g \sim \pi_h} \left[\gamma^{ik} \left(\sum_{j=0}^{k-1} \gamma^j \mathbb{E}_{s, a \sim \mathbb{P}_{ik+j}^{\pi_l, g}(\cdot, \cdot | s_0)} r(s_{ik+j}, a_{ik+j}, \hat{g}) \right) \right] \\ &= \sum_{j=0}^{k-1} \mathbb{E}_{g \sim \pi_h, s, a \sim \mathbb{P}_j^{\pi_l, g}(\cdot, \cdot | s_0)} [\gamma^j r(s_j, a_j, \hat{g})] \\ &\quad + \sum_{i=1}^{\infty} \mathbb{E}_{g \sim \pi_h} \left[\gamma^{ik} \left(\sum_{j=0}^{k-1} \gamma^j \mathbb{E}_{s, a \sim \mathbb{P}_{ik+j}^{\pi_l, g}(\cdot, \cdot | s_0)} r(s_{ik+j}, a_{ik+j}, \hat{g}) \right) \right] \\ &= \tilde{V}_0^{\pi_h, \pi_l}(s_0) + \gamma^k \mathbb{E}_{g \sim \pi_h, s \sim \mathbb{P}_k^{\pi_l, g}(\cdot | s_k)} [V^{\pi_h, \pi_l}(s_k)]. \end{aligned} \quad (38)$$

Thus, we can conclude that

$$V^{\pi_h, \pi_l}(s_{ik}) = \tilde{V}_i^{\pi_h, \pi_l}(s_{ik}) + \gamma^k \mathbb{E}_{g \sim \pi_h, s \sim \mathbb{P}_{(i+1)k}^{\pi_l, g}(\cdot | s_{ik})} [V^{\pi_h, \pi_l}(s_{(i+1)k})]. \quad (39)$$

And the proof is complete. \square

Lemma A.4 (Markov chain TVD bound, time-varying). *Suppose the expected KL-divergence between two policy distributions is bounded as $\epsilon_{\pi_l^*, \pi_l}^g = \max_{s \in \mathcal{S}, g \sim \pi_h} \mathbb{D}_{TV}(\pi_l^*(\cdot | s, g) \| \pi_l(\cdot | s, g))$, and the initial state distributions are the same. Then, the distance in the state-action marginal is bounded as,*

$$\mathbb{D}_{TV} \left(\mathbb{P}_t^{\pi_l^*, g}(\cdot, \cdot | s_0) \middle\| \mathbb{P}_t^{\pi_l, g}(\cdot, \cdot | s_0) \right) \leq t \epsilon_{\pi_l^*, \pi_l}^g \quad (40)$$

Proof. Let $p(s' | s)$ as the adjacent state transition probability, which can be defined as

$$p(s' | s) = p(s) P(s' | s, a) \pi(a | s). \quad (41)$$

Replacing the policy as the low-level policy π_l , we can derive the Markov chain TVD bound caused by the different low-level policy,

$$\begin{aligned} &\max_t \mathbb{E}_{s \sim p_1^t(s)} \mathbb{D}_{KL}(p_1(s' | s) \| p_2(s' | s)) \\ &= \max_t \mathbb{E}_{s \sim p_1^t(s)} p(s) P_{s, s'}^a(s' | s, a) \mathbb{D}_{KL}(\pi_l^*(a | s, g) \| \pi_l(a | s, g)) \\ &\leq \max_t \mathbb{E}_{s \sim p_1^t(s)} \mathbb{D}_{KL}(\pi_l^*(a | s, g) \| \pi_l(a | s, g)) \\ &\leq \max_{s \in \mathcal{S}, g \sim \pi_h} \mathbb{D}_{TV}(\pi_l^*(\cdot | s, g) \| \pi_l(\cdot | s, g)) \\ &= \epsilon_{\pi_l^*, \pi_l}^g \end{aligned} \quad (42)$$

Thus, follow the Lemma B.2 in Janner et al. (2019), the distance in the state-action marginal is bounded as,

$$\mathbb{D}_{TV} \left(\mathbb{P}_t^{\pi_l^*, g}(\cdot, \cdot | s_0) \middle\| \mathbb{P}_t^{\pi_l, g}(\cdot, \cdot | s_0) \right) \leq t \epsilon_{\pi_l^*, \pi_l}^g. \quad (43)$$

And the proof is complete. \square

Assumption A.5 (Refer to Assumption 1 in [Zhang et al. \(2022\)](#)). For all $s \in \mathcal{S}$ and $g \in \mathcal{G}$, the environmental reward can be written as

$$r(s, a, \hat{g}) = \sum_{s'} P_{s,s'}^a(s'|s, a) \pi_l(a|s, g) \tilde{r}(s, s') = \mathbb{E}_{g \sim \pi_h, s, a \sim \mathbb{P}_t^{\pi_l, g}} r_l(s_t, a_t, g) / \mathcal{D}(g, \hat{g}). \quad (44)$$

where $\tilde{r} : \mathcal{S} \times \mathcal{G} \rightarrow [0, r_{max}]$ is a state-reachability reward function.

In this assumption, the subgoal g generated by the high-level policy represents the desired state to be reached, while the intermediate low-level state and action details are controlled by the low-level policy. Therefore, considering that the subgoals are generated towards the environmental goal \hat{g} , when given a low-level optimal/learned policy, it is natural to assume that the k -step stage reward only depends on the state where the agent starts and the state where the agent arrives.

B Experimental Details

B.1 Implementation Details

Our method BrHPO and all baselines are implemented based on PyTorch.

BrHPO. We employ the soft actor-critic (SAC) algorithm [Haarnoja et al. \(2018b\)](#) as the backbone framework for both high- and low-level policies. For the high-level policy, considering that the subtask trajectory $\tau_i^{\pi_h, \pi_l}$ in each subtask would be abstracted as one transition in high level, we convert the trajectory $(s_{ik:(i+1)k-1}, a_{ik:(i+1)k-1}, g_{(i+1)k}, r_{h,ik}, s_{(i+1)k})$ into a high-level transition tuple $(s_{ik}, g_{(i+1)k}, r_{h,ik}, s_{(i+1)k})$. Then, when a subtask ends, we compute the subgoal reachability by

$$\mathcal{R}_i^{\pi_h, \pi_l} = \mathbb{E}_{r_l \sim \tau_i^{\pi_h, \pi_l}} \frac{r_{l,(i+1)k}}{r_{l,ik}}.$$

Then, we can optimize the high-level policy by

$$Q^{\pi_h}(s, g) = \arg \min_Q \frac{1}{2} \mathbb{E}_{s, g \sim D_h} [r_h(s, g) + \gamma \mathbb{E}_{s' \sim D_h, g' \sim \pi_h} Q^{\pi_h}(s', g') - Q^{\pi_h}(s, g)]^2,$$

$$\pi_h = \arg \min_{\pi_h} \mathbb{E}_{s \sim D_h} [\text{D}_{KL}(\pi_h(\cdot|s) \| \exp(Q^{\pi_h}(s, g) - V^{\pi_h}(s))) + \lambda_1 \mathcal{R}_i^{\pi_h, \pi_l}].$$

For the low-level policy which can be trained as a goal-conditioned one, we design the reachability-aware low-level policy as

$$\hat{r}_l(s_{ik+j}, a_{ik+j}, g_{(i+1)k}) = r_l(s_{ik+j}, a_{ik+j}, g_{(i+1)k}) - \lambda_2 \mathcal{R}_i^{\pi_h, \pi_l}.$$

The training tuples for the low-level policy are formed as the per-step state-action transitions $(s_{ik+j}, g_{(i+1)k}, a_{ik+j}, r_{l,ik+j}, s_{ik+j+1}, g_{(i+1)k})$ ¹, which then are stored in the low-level buffer D_l . Thus, with the training tuples, we can optimize the low-level policy as,

$$Q^{\pi_l}(s, a) = \arg \min_Q \frac{1}{2} \mathbb{E}_{s, g, a \sim D_l} [\hat{r}_l(s, a, g) + \gamma \mathbb{E}_{s', g \sim D_l, a' \sim \pi_l} Q^{\pi_l}(s', a') - Q^{\pi_l}(s, a)]^2,$$

$$\pi_l = \arg \min_{\pi_l} \mathbb{E}_{s, g \sim D_l} [\text{D}_{KL}(\pi_l(\cdot|s, g) \| \exp(Q^{\pi_l}(s, a) - V^{\pi_l}(s)))].$$

Algorithm framework. We briefly give an overview of our proposed BrHPO in [algorithm 1](#). Notably, the mutual response mechanism effectively calculates the subgoal reachability for bilateral information and then incorporates it into hierarchical policy optimization for mutual error correction, promoting performance and reducing computation load.

HIRO. In this work [Nachum et al. \(2018b\)](#), to deal with the non-stationarity, where old off-policy experience may exhibit different transitions conditioned on the same goals, they heuristically relabel the subgoal \tilde{g} as

$$\log \mu^{lo}(a_{t:t+c+1} | s_{t:t+c+1}, \tilde{g}_{t:t+c+1}) \propto -\frac{1}{2} \sum_{i=t}^{t+c-1} \|a_i - \mu^{lo}(s_i, \tilde{g}_i)\|_2^2 + \text{const}.$$

To solve this problem efficiently, they calculated the quantity on eight candidate goals sampled randomly from a Gaussian centred at $s_{t+c} - s_t$. Then, with the correcting high-level experience, the high-level policy can be optimized by off-policy methods. Compared with our methods, the off-correction can be regarded as a low-level domination method, which requires the high-level experience to be modified by the subgoal reachability demonstrated at a low level.

¹We use the absolute subgoal in this paper, that is, $g_{(i+1)k} = s_{ik} + \pi_h(\cdot|s_{ik})$.

Algorithm 1 Bidirectional-reachable Hierarchical Policy Optimization (BrHPO)

```

initialize: policy networks  $\pi_h, \pi_l$ ,  $Q$ -networks  $Q^{\pi_h}, Q^{\pi_l}$ , replay buffers for high-level  $D_h$  and
low-level  $D_l$ 
for each training episode do
  while not done do
    sample subgoals  $g \sim \pi_h(\cdot|s)$ 
    for each step in a subtask do
      Sample actions  $a \sim \pi_l(\cdot|s, g)$ 
      Store  $(s, g, a, r_l, s', g)$  into a temp buffer
      Update  $\pi_l$  by (9) and (10) from  $D_l$  ▷ low-level policy optimization
    end for
    Calculate  $\mathcal{R}_i^{\pi_h, \pi_l}$  by (5) ▷ subgoal reachability computation
    Compute  $\hat{r}_l$  by (8) and push the tuples in  $D_l$  ▷ reachability-aware low-level reward
    Store  $(s, g, r_h, s', \hat{\mathcal{R}}_i^{\pi_h, \pi_l})$  into  $D_h$ 
    Update  $\pi_h$  by (6) and (7) from  $D_l$  ▷ high-level policy optimization
  end while
end for

```

HIGL. In this work Kim et al. (2021), to restrict the high-level action space from the whole goal space to a k -step adjacent region, they introduced the shortest transition distance as a constraint in high-level policy optimization. Besides, they utilized farthest point sampling and priority queue \mathcal{Q} to improve the subgoal coverage and novelty. To enhance the subgoal reachability, they made pseudo landmark be placed between the selected landmark and the current state in the goal space as follows:

$$g_t^{\text{pseudo}} := g_t^{\text{cur}} + \delta_{\text{pseudo}} \cdot \frac{g_t^{\text{sel}} - g_t^{\text{cur}}}{\|g_t^{\text{sel}} - g_t^{\text{cur}}\|^2}.$$

To establish the adjacency constraint by the shortest transition distance, they refer to HRAC Zhang et al. (2020) and adopt an adjacent matrix to model it. Specifically, we note that the performance of HIGL in the AntMaze task is different from the original report in their paper, mainly due to the different scales. Thus, we set the same scale for all tasks for fairness. To ensure that HIGL performs well in these tasks, we adjusted hyper-parameters such as "landmark coverage" and "n landmark novelty".

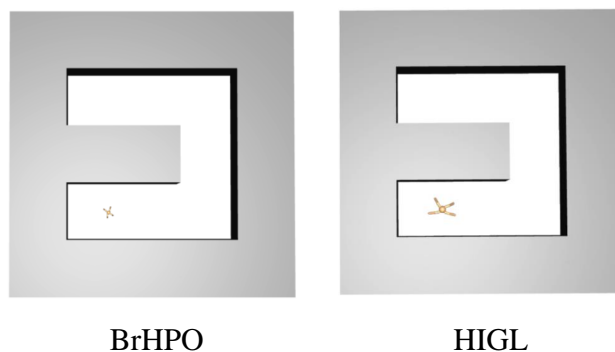


Figure 10: Comparison of the scales in the maze tasks between BrHPO and HIGL.

CHER. This work Kreidieh et al. (2019) proposed a cooperation framework for HRL. In this work, the HRL problem can similarly be framed as a constrained optimization problem,

$$\max_{\pi_m} \left[J_m + \min_{\lambda \leq 0} \left(\lambda \delta - \lambda \min_{\pi_w} J_w \right) \right].$$

To deal with this problem, they update the high- (π_m) and low-level (π_w) policies by

$$\theta_w \leftarrow \theta_w + \alpha \nabla_{\theta_w} J_w, \quad \text{and}, \quad \theta_m \leftarrow \theta_m + \alpha \nabla_{\theta_w} (J_w + \lambda J_w).$$

Compared to CHER, our BrHPO method distinguishes itself in several key aspects. In CHER, hierarchical cooperation is achieved solely through high-level policy optimization, while the low-level policy is trained as a generally goal-conditioned policy without further improvement. Moreover, the high-level optimization in CHER introduces J_w as $(J_w + \lambda J_w)$, necessitating a focus on the step-by-step behaviour of the low-level policy.

In contrast, our BrHPO method incorporates the concept of subgoal reachability, which considers the initial and final states of the subtasks. This design choice empowers the high-level policy to relax the exploration burden on the low-level policy. By leveraging subgoal reachability, our approach enables more efficient exploration of the low-level policy and facilitates effective hierarchical cooperation between the high-level and low-level policies.

RIS. In this work [Chane-Sane et al. \(2021\)](#), based on the hindsight method, they collected feasible state trajectories and predicted an appropriate distribution of imagined subgoals. They first defined subgoals s_g as midpoints on the path from the current state s to the goal g , and further minimized the length of the paths from s to s_g and s_g to g . Thus, the high-level policy can be updated as

$$\pi_{k+1}^H = \arg \min_{\pi^H} \mathbb{E}_{(s,g) \sim D, s_g \sim \pi^H(\cdot|s,g)} [C_{\pi}(s_g|s, g)].$$

Then, with the imagined subgoals, the low-level policy can be trained by

$$\pi_{\theta_{k+1}} = \arg \max_{\theta} \mathbb{E}_{(s,g) \sim D} \mathbb{E}_{a \sim \pi_{\theta}(\cdot|s,g)} \left[Q^{\pi}(s, a, g) - \alpha D_{KL} \left(\pi_{\theta} \| \pi_k^{prior} \right) \right].$$

B.2 Network Architecture

For the hierarchical policy network, we employ SAC [Haarnoja et al. \(2018b\)](#) as both the high-level and the low-level policies. Each actor and critic network for both high level and low level consists of 3 fully connected layers with ReLU nonlinearities. The size of each hidden layer is (256, 256). The output of the high- and low-level actors is activated using the linear function and is scaled to the range of corresponding action space.

We use Adam optimizer [Kingma & Ba \(2014\)](#) for all networks in BrHPO.

B.3 Environmental Setup

We adopt six challenging long-term tasks to evaluate BrHPO, which can be categorized into the *dense* case and the *sparse* case. For the maze navigation tasks, a simulated ant starts at (0, 0) and the environment reward is defined as $r = -\sqrt{(x - g_x)^2 + (y - g_y)^2}$ (except for AntFall, $r = -\sqrt{(x - g_x)^2 + (y - g_y)^2 + (z - g_z)^2}$). While in the robotics manipulation tasks, a manipulator is initialized with a horizontal stretch posture. The environmental reward is defined as a binary one, determined by the distance between the end-effector (or the object in Pusher) and the target point

$$r = \begin{cases} -1, & d > 0.25, \\ 0, & d \leq 0.25. \end{cases} \quad (45)$$

And, the success indicator is defined as whether the final distance is less than a pre-defined threshold, where the maze navigation tasks require $d < 5$ and the robotics manipulation tasks require $d < 0.25$.

AntMaze. A simulated eight-DOF ant starts from the left bottom (0, 0) and needs to approach the left top corner (0, 16). At each training episode, a target position is sampled uniformly at random from $g_x \sim [-4, 20]$, $g_y \sim [-4, 20]$. At the test episode, the target points are fixed at $(g_x, g_y) = (0, 16)$.

AntBigMaze. Similar to the AntMaze task, we design a big maze to evaluate the exploration capability of BrHPO. In particular, the target position is chosen randomly from one of $(g_x, g_y) = (32, 8)$ and $(g_x, g_y) = (66, 0)$, which makes it harder to find a feasible path.

AntPush. A movable block at $(0, 8)$ is added to this task. The ant needs to move to the left side of the block and push it into the right side of the room, for a chance to reach the target point above, which requires the agent to avoid training a greedy algorithm. At each episode, the target position is fixed to $(g_x, g_y) = (0, 19)$.

AntFall. In this task, the agent is initialized on a platform of height 4. Like the AntPush environment, the ant has to push a movable block at $(8, 8)$ into a chasm to create a feasible road to the target, which is on the opposite side of the chasm, while a greedy policy would cause the ant to walk towards the target and fall into the chasm. At each episode, the target position is fixed to $(g_x, g_y, g_z) = (0, 27, 4.5)$.

Reacher3D. A simulated 7-DOF robot manipulator needs to move its end-effector to a desired position. The initial position of the end-effector is at $(0, 0, 0)$ while the target is sampled from a Normal distribution with zero mean and 0.1 standard deviation.

Pusher. Pusher additionally includes a puck-shaped object based on the Reacher3D task, and the end-effector needs to find the object and push it to a desired position. At the initialization, the object is placed randomly and the target is fixed at $(g_x, g_y, g_z) = (0.45, -0.05, -0.323)$.

We summarise these six tasks in Table 1.

Table 1: Overview on Environment settings.

Environment	state	action	environment reward	episode step	success indicator
AntMaze	32	8	negative x-y distance	500	$r_{\text{final}} \geq -5$
AntBigMaze	32	8	negative x-y distance	1000	$r_{\text{final}} \geq -5$
AntPush	32	8	negative x-y distance	500	$r_{\text{final}} \geq -5$
AntFall	33	8	negative x-y-z distance	500	$r_{\text{final}} \geq -5$
Reacher3D	20	7	negative x-y-z distance	100	$d_{\text{final}} \leq 0.25$
Pusher	23	7	negative x-y-z distance	100	$d_{\text{final}} \leq 0.25$

B.4 Hyper-parameters

Table 2 lists the hyper-parameters used in training BrHPO over all tasks.

C Additional experiments

Additional Metrics. We report additional (aggregate) performance metrics of BrHPO and other baselines on the six tasks using the `rliable` toolkit Agarwal et al. (2021). As show in Figure 11, BrHPO outperforms other baselines in terms of Median, interquantile mean (IQM), Mean and Optimality Gap results.

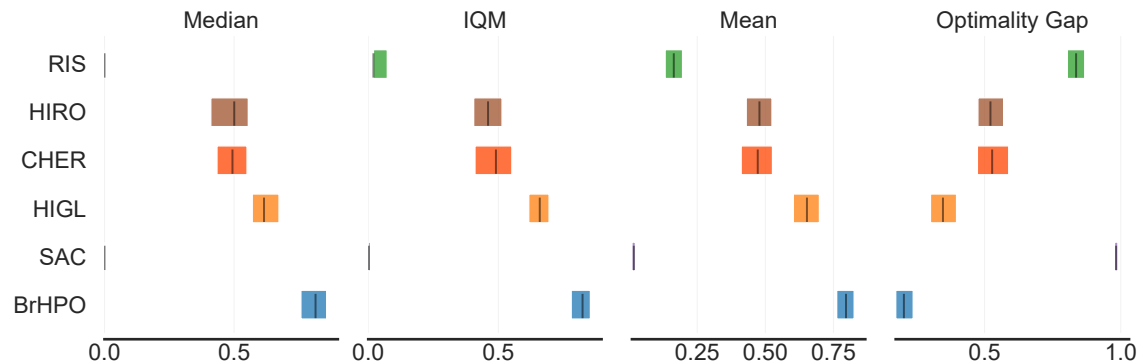


Figure 11: Median, IQM, Mean (higher values are better) and Optimality Gap (lower values are better) performance of BrHPO and all baselines on six tasks.

Subgoal reachability report. We report the average subgoal reachability $\mathcal{R}_i^{\pi_h, \pi_l}$ of each environment by Table 3. Note that, the value $\mathcal{R}_i^{\pi_h, \pi_l} \rightarrow 0$ means the final distance $\mathcal{D}(\psi(s_{(i+1)k}), g_{(i+1)k}) \rightarrow 0$, thus implying the better subgoal reachability. From the results, our implementation is simple yet effective, which can improve subgoal reachability significantly. Besides, the results show that when there are contact dynamics in the environment, such as AntPush, AntFall and Pusher, the subgoal reachability may be decreased, which inspires us to further develop investigation in these cases.

Ablation by the sparse environment. Additionally, we provide ablation studies conducted on the Reacher3D task (*sparse*) instead of the AntMaze task (*dense*). We investigate the effectiveness of the mutual response mechanism by 1) the three variants of BrHPO, containing *Vanilla*, *NoReg* and *NoBonus*, and 2) the weighted factors λ_1 and λ_2 . We show the results in Figure 12. Overall, we find that the tendency from the Reacher3D task is similar to the AntMaze task, which verifies the effectiveness of our BrHPO in the *sparse* reward case.

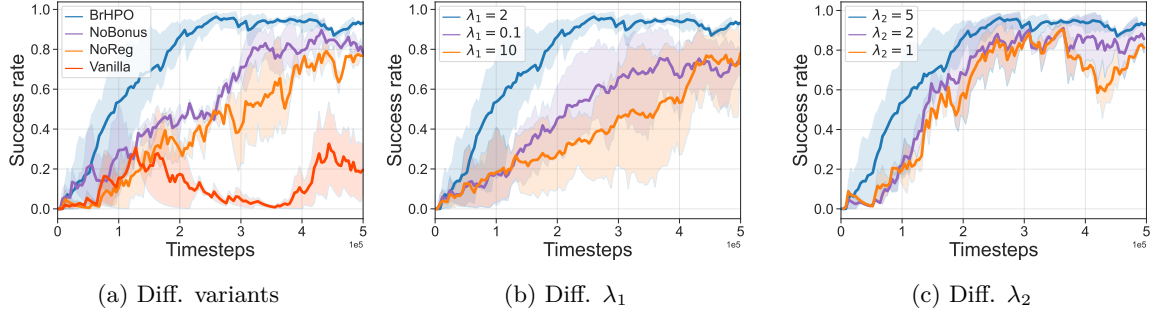


Figure 12: The ablation of mutual response mechanism by Reacher3D task. Mean and std by 4 runs.

Empirical study in stochastic environments. To empirically verify the stochasticity robustness of BrHPO, we utilize it the a set of stochastic tasks, including stochastic AntMaze, AntPush and Reacher3D, which are modified from the original tasks. Referring to HRAC Zhang et al. (2020), we interfere with the position of the ant (x,y) and the position of the end-effector (x,y,z) with Gaussian noise of different standard deviations, including $\sigma = 0.01$, $\sigma = 0.05$ and $\sigma = 0.1$, to verify the robustness against the increasing environmental stochasticity. As shown in Figure 13, BrHPO can achieve similar asymptotic performance with different noise magnitudes in stochastic AntMaze, AntPush and Reacher3D, which shows the robustness to stochastic environments.

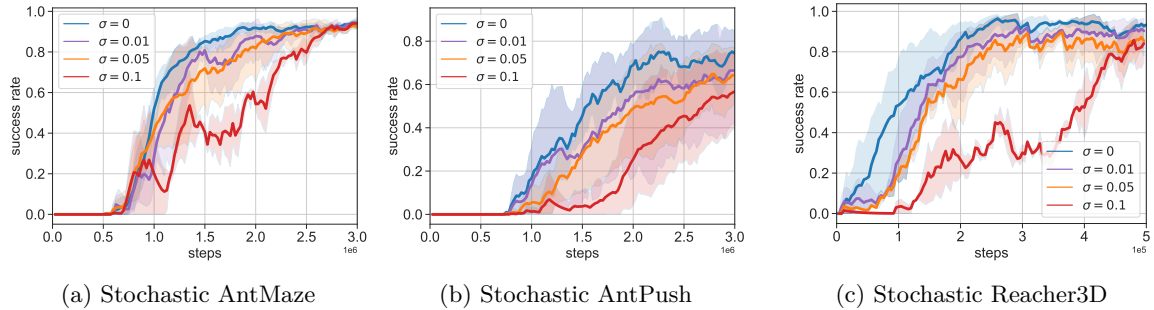


Figure 13: The empirical evaluation of BrHPO by stochastic environments. Mean and std by 4 runs.

C.1 Computing Infrastructure and Training Time

For completeness, we list the computing infrastructure and benchmark training times for BrHPO and all baselines by Table 4. As discussed in section 4.2, the training complexity of BrHPO is much less than other HRL methods, which can be comparable to the flat policy.

Table 2: The hyper-parameters settings for BrHPO.

	AntMaze	AntBigMaze	AntPush	AntFall	Reacher3D	Pusher
Q -value network (both high and low)	MLP with hidden size 256					
policy network (both high and low)	Gaussian MLP with hidden size 256					
discounted factor γ	0.99					
soft update factor τ	0.005					
Q -network learning rate	0.001					
policy network learning rate	0.0001					
automatic entropy tuning (high-level)	False		True		False	
automatic entropy tuning (low-level)	False					
batch size	128					
update per step	1					
target update interval	2					
high-level replay buffer	1e5					
low-level replay buffer	1e6					
start steps	5e3					
subtask horizon	20			10		
reward scale	1					
high-level responsive factor λ_1	2		0.5		2	
low-level responsive factor λ_2	10			5		

Table 3: The average subgoal reachability of BrHPO.

Environment	AntMaze	AntBigMaze	AntPush	AntFall	Reacher3D	Pusher
subgoal reachability	0.22	0.29	0.33	0.32	0.13	0.18

Table 4: Computing infrastructure and training time on each task (in hours).

	AntMaze	AntBigMaze	AntPush	AntFall	Reacher3D	Pusher
CPU	AMD EPYC™ 7763					
GPU	NVIDIA GeForce RTX 3090					
HIRO	16.66	23.14	18.29	25.43	3.42	4.25
HIGL	31.59	48.45	30.95	49.60	5.96	7.05
CHER	15.38	20.53	16.71	21.37	2.96	3.16
RIS	40.83	53.49	38.46	57.05	8.63	9.88
SAC	10.57	11.36	11.75	15.64	2.35	2.68
BrHPO	12.75	18.74	13.43	19.17	2.73	3.53
comparison (Ours - SAC)	2.18	7.38	1.68	3.53	0.38	0.85